Single-particle characterization of polycyclic aromatic hydrocarbons in background air in Northern Europe

Johannes Passig[1,2,3], Julian Schade[1,2,5], Robert Irsig[1,2,4], Thomas Kröger-Badge[1,2], Hendryk Czech[1,2,3], Thomas Adam[3,5], Henrik Fallgren[6], Jana Moldanova[6], Martin Sklorz[3], Thorsten Streibel[1,3], and Ralf Zimmermann[1,2,3]

[1]Joint Mass Spectrometry Centre, Chair of Analytical Chemistry, University Rostock, 18059 Rostock, Germany
[2]Department Life, Light & Matter, University of Rostock, 18059 Rostock, Germany
[3]Joint Mass Spectrometry Centre, Cooperation Group 'Comprehensive Molecular Analytics' (CMA), Helmholtz Zentrum München, 81379 München, Germany
[4]Photonion GmbH, 19061 Schwerin, Germany
[5]Bundeswehr University Munich, 85577 Neubiberg, Germany
[6]IVL Swedish Environmental Research Institute, 411 33 Gothenburg, Sweden

Correspondence to: Johannes Passig (johannes.passig@uni-rostock.de)

Abstract. We investigated the distribution of polycyclic aromatic hydrocarbons (PAH) on individual ambient aerosol particles at the Swedish west coast in a pristine environment for ten days in October 2019. The measurements were carried out using new technology in single-particle mass spectrometry (SPMS) that reveals both the inorganic particle composition as well as the particle-bound PAHs (Schade et al., 2019). More than 290,000 particles were characterized; 4,412 of them reveal PAH signatures. Most of the PAH-containing particles were internal mixtures of carbonaceous material, secondary nitrate, and metals from distant sources in Central and Eastern Europe. We characterize the aerosol with respect to the inorganic composition, comparable to conventional SPMS before we discuss the distribution of PAHs within this particle ensemble. Vice versa, we analyze the single-particle PAH spectra for characteristic patterns and discuss the inorganic composition, origin, and atmospheric processing of the respective particles. The study period comprised different meteorological situations: clean air conditions with winds from the North Sea/Kattegat and little terrestrial air pollution, long-range transport from Eastern Europe and southern Sweden as well as transport of aerosols from Central Europe over the sea. For all meteorological conditions, PAHs were detected in particles whose inorganic content indicates traffic emissions, such as combinations of soot, iron, and calcium as well as in particles with biomass burning signatures. However, there were variations in their amounts, dependent on the geographic origin. Because of strong mixing, rapid degradation, and speciation limits, e.g. for PAHs of the same nominal mass, the application of diagnostic ratios for source apportionment is limited under the conditions of our study. Nevertheless, the combination with the inorganic content and meteorological data provide unique insight into the particles' origin, aging, and mixing state. We exemplarily show how the observation of PAH profiles and inorganic secondary components on a single-particle level can open a new door to investigate aerosol aging processes. To our best knowledge, we herewith present the first comprehensive study on the single-particle distribution of PAHs in ambient air as well as the first set of combined data on PAHs and inorganic composition on a single-particle level.

1 Introduction

Polycyclic aromatic hydrocarbons (PAHs) are ubiquitous organic trace components in atmospheric aerosols. They are released into the atmosphere by all types of natural and anthropogenic combustion processes. Because of their well-documented carcinogenicity and mutagenicity, they play a key role in health effects from air pollution (Kim et al., 2013; Agudelo-Castañeda

et al., 2017). After entering the atmosphere, PAHs are widely distributed by aerosols before being deposited onto soils, water, and vegetation (Ravindra et al., 2008; Dat and Chang, 2017). Estimates of the impact of particular sources, the distribution pathways, and the degradation processes are crucial for risk assessment. Measurements of PAHs in the atmosphere are typically based on filter sampling and subsequent analysis via gas chromatography techniques (Pandey et al., 2011; Nozière et al., 2015). PAHs are emitted as a mixture and their relative concentration ratios are assumed to be characteristic of a particular source (Ravindra et al., 2008; Tobiszewski and Namieśnik, 2012; Dat and Chang, 2017; Czech et al., 2017). Consequently, pairs of PAHs with comparable physicochemical properties are often analyzed for source apportionment. However, most of these diagnostic ratios are not stable, for example, because of different decay ratios for photolysis reactions during atmospheric aging (Vione et al., 2006; Tobiszewski and Namieśnik, 2012). Also, numerous interactions with other aerosol components that affect PAH degradation are discussed (Keyte et al., 2013), e.g. shielding of PAHs against oxidants by organic coatings (Zelenyuk et al., 2017; Shrivastava et al., 2017; Alpert et al., 2021). Detailed information on the PAH-containing particles, such as their inorganic composition, mixing state or morphology might substantially improve source attribution and degradation estimates. Beyond that, the occurrence and distribution of PAHs are highly variable as human activity and meteorological conditions change rapidly. Assessments of the exposure and environmental impact would therefore benefit from real-time monitoring.

Several aerosol mass spectrometers can obtain chemical information from airborne particles in real-time (Pratt and Prather, 2012; Laskin et al., 2018). Among these techniques, single-particle mass spectrometry (SPMS) stands out for characterizing individual particles, thus revealing the mixing state of the particle ensemble (Murphy, 2007; Hinz and Spengler, 2007; Riemer et al., 2019; Passig and Zimmermann, 2020). In conventional SPMS, individual particles are hit by intense laser radiation that desorbs and ionizes at least a fraction of the particle within a single laser pulse (laser desorption/ionization, LDI). This ionization technique is highly non-linear; ionization efficiencies of particle compounds vary widely and depend also on the particle's main components and morphology (Neubauer et al., 1998; Murphy, 2007; Reinard and Johnston, 2008; Hatch et al., 2011; Hatch et al., 2014). However, LDI produces sufficient ion numbers even from single nanoparticles (Wang et al., 2006) and is also effective for refractory compounds like metals (Murphy et al., 2006; Dall'Osto et al., 2016b; Arndt et al., 2017; Dall'Osto et al., 2016a; Passig et al., 2020). Besides its relevance for the environment and health, the refractory components are typically conserved and bear particle source information that can exclusively be addressed by SPMS.

In contrast to metals or salts, the speciation of organic species in LDI-based SPMS is limited by strong fragmentation of molecules in the intense UV laser pulse. Only for specific particle matrices such as rather pure carbon (i.e. soot particles), molecular PAHs are sufficiently detectable by LDI-MS (Zimmermann et al., 2003). Therefore, several approaches for "soft" ionization of molecules from the particles have been developed, namely single-photon ionization, SPI (Sykes et al., 2002; Nash et al., 2005; Hanna et al., 2009), and resonance-enhanced multiphoton ionization (REMPI) (Morrical et al., 1998; Bente et al., 2008, 2009; Li et al., 2019). The latter is especially suitable for SPMS because it is highly specific and very sensitive to PAHs (Boesl, 2000; Gunzer et al., 2019), thus capable to detect this particularly relevant substance group on a single-particle basis. The typical REMPI (and SPI) approach is a two-step scheme, where an IR laser pulse heats the particle and produces a gaseous

plume of the organic molecules prior to the UV ionization pulse (laser desorption, LD-REMPI). Vaporization of molecules before ionization also avoids some of the matrix effects associated with single-step LDI and can thus facilitate quantification (Woods et al., 2001). Only a limited number of such two-step approaches were applied for real-world ambient aerosols (Zelenyuk and Imre, 2005; Bente et al., 2008; Oster et al., 2011) and they have the important disadvantage that the inorganic particle composition from LDI, and thus the particle source information, is lost.

Recently, this limitation was overcome by methods that combine LDI and LD-REMPI (Passig et al., 2017; Schade et al., 2019), detecting positive and negative ions from LDI similar to conventional SPMS together with full-fledged mass spectra of PAHs via REMPI (Schade et al., 2019). Briefly, a special laser pulse profile is utilized to ionize PAHs after LD from the refractory particle residue, while the latter is hit by a more intense part of the beam, thus inducing LDI and REMPI within a single laser shot. Furthermore, the mass analyzer's transmission is modulated with respect to the different ionization products to achieve sufficient sensitivity and dynamic range.

Here we report on the first field study using this technique and present the first set of single-particle data on PAHs combined with information on the particle class and origin as derived from the inorganic composition.

2 Methods

2.1 SPMS instrumentation

The SPMS instrument comprises two reflectron time-of-flight mass analyzers (Stefan Kaesdorf GmbH) and corresponds to the ATOF-MS technique (Prather et al., 1994; Hinz et al., 1994). Its working principle and parameters have been described in detail previously (Schade et al., 2019) and were not changed. Briefly, the particles are introduced through an aerodynamic lens, detected and sized via light scattering using a pair of continuous wave-lasers (wavelength λ= 532 nm) and photomultipliers before entering the mass spectrometer. Shortly before the center of the ion source, the particles are exposed to an IR pulse for laser desorption (λ= 10.6 µm). A few microseconds later, a parallel UV beam from an excimer laser (λ= 248 nm) intersects the gaseous plume with moderate intensity (~3 MW/cm^2), ionizing the desorbed PAHs via REMPI. The beam is then back-reflected and focused with a concave mirror and hits the particle residue in the plume center with a high intensity (~2 GW/cm^2) inducing LDI of the refractory components. Cations from LDI are detected together with the PAH-ions from REMPI in the positive tube of the Time-of-Flight (TOF) mass analyzer and anions from LDI are measured in the negative TOF-tube. To achieve the large dynamic range for measuring the high ion flux from LDI and the much lower signals from REMPI with the same detector, the transmission of the positive flight tube is attenuated by a factor of about 50 for the lighter LDI ions. All ions are extracted with a delay of 0.6 µs after the ionization pulse to improve the quality of mass spectra (Vera et al., 2005; Li et al., 2018). The TOF is tuned to achieve a sufficient mass resolution of about R ≈ 800…1000 for both low-mass ions from LDI and high-mass ions from REMPI. Particle sizing signals and ion TOF data were recorded by custom LabView software.

2.2 Analysis of single-particle mass spectra

A custom software on the Matlab platform (MathWorks Inc.) was used to compute mass spectra from time-of-flight data considering peak area within nominal mass resolution. Mass spectra from positive and negative LDI as well as from REMPI were separately normalized. For clustering, we used the adaptive resonance theory neural network, ART-2a (Carpenter et al., 1991; Song et al., 1999), publicly available with the open-source toolkit FATES (Flexible Analysis Toolkit for the Exploration of SPMS data) (Sultana et al., 2017). Of note, the ionization process, as well as the data structure from LDI and REMPI mass spectra differ substantially. PAH patterns appear as peak rows, bearing information in the intensity distribution of many high-mass peaks, which can in most cases not be unequivocally attributed to specific compounds. LDI signals show fewer peaks that are often assignable to particle components. Consequently, we performed independent clustering for LDI and REMPI mass spectra and characterized the LDI-based clusters concerning their PAH content. Vice versa, we studied the REMPI-based clusters for their inorganic composition via LDI. Clustering parameters for LDI clustering were chosen as 'standard values' with a learning rate of 0.05, a vigilance factor of 0.8, and 20 iterations. For REMPI clustering, the vigilance factor was 0.7, a value that resulted in a good balance between the number of clusters that can be evaluated in manual regrouping and the recognition of prominent PAH signatures. LDI ion peaks were assigned to the most likely ion at a given mass (m/z).

2.3 Measurement site and aerosol sampling

The experiments were performed at a monitoring station in a rural environment at the Swedish west coast, about 35 km south of Gothenburg (coordinates 57°23'37.8"N, 11°54'51.4"E). The site belongs to the Onsala Space Observatorium, which is located on a peninsula with restricted access and nearly no traffic, residential or industrial emissions nearby, see Fig. 1. Ambient air was sampled at 7 m height above ground (20 m above sea level). The low concentration of background aerosols required enrichment technology. Therefore, an aerosol concentrator, was used (Model 4240, MSP corp., USA) (Romay et al., 2002) that concentrates particles from the 300 l/min intake airflow into a 1 l/min carrier gas stream. After passing a dryer (Model MD-700-12S-1, Perma Pure LLC, U.S.) the aerosols were further concentrated to 0.1 l/min using an additional virtual impactor stage at the SPMS aerodynamic lens inlet (Zhuo et al., 2021). The first concentrator was designed for particles larger than 1 µm, therefore the system's total concentration factor for ambient air particles around 0.5 µm size is approximately 10:1 and rapidly drops to 1 below 0.5 µm, as estimated in a previous study (Passig et al., 2020). Because of the limited detection efficiency for particles below ~150 nm size in SPMS (Su et al., 2004; Zelenyuk et al., 2009) and the size-dependent enrichment factor in this experiment, our study targets on long-range transported particles rather than the ultra-fine size mode.

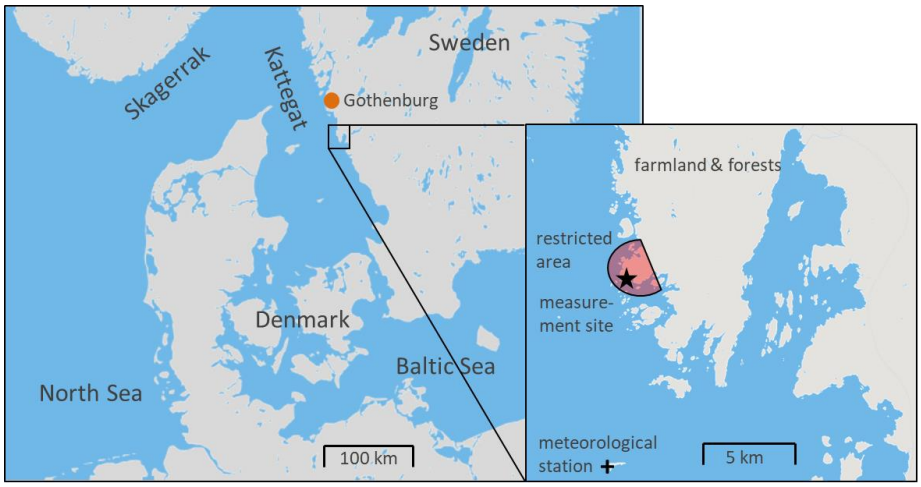

Figure 1: Map of the region and position of the measurement site at the Swedish west coast.

Aerosol mass concentration was measured with an optical particle counter (Grimm EDM-180 MC) that belongs to the standard instrumentation of the station. Meteorological data was acquired from the Swedish Meteorological and Hydrological Institute, station Nidingen, located on an island 8 km south of the sampling site (SMHI, 2021). Air back trajectories were computed using the HYSPLIT web tool from the National Oceanic and Atmospheric Administration, model GFS with 0.25° resolution (http://www.ready.noaa.gov/HYSPLIT.php, last access 11 January 2021) (Stein et al., 2015).

3. Results and Discussion

3.1 Main particle classes from conventional analysis of LDI mass spectra

Before focusing on the particle-bound PAHs, we describe the aerosol ensemble according to the usual practice of conventional LDI-based SPMS. Between the 12th and the 22nd of October 2019, a total number of about 1 million individual particles were optically detected and sized, whereof 292,242 were analyzed with respect to their chemical composition by at least one mass spectrum (minimum of four peaks) from either anions from LDI, cations from LDI or PAHs from REMPI. The ART-2a clustering of LDI signatures yielded 892 clusters. The top 300 clusters account for 86 % of the analyzed particles and were visually inspected. Clusters with the same overall species and comparable trends and size distributions were manually merged to 10 general particle classes. Thus, clusters resulting from mass spectral artefacts such as occasional peak broadening or saturation can be evaluated as well as potentially interesting minor clusters. The abundances and mean aerodynamic sizes of the general classes are shown in Fig. 2(a), while Fig. 2(b) shows their respective LDI mass spectra. The labelling scheme indicates the most intense peaks and characteristic composition, see also (Ault et al., 2010; Decesari et al., 2014; Dall'Osto et

al., 2016a; Arndt et al., 2017). The mass spectral signatures of the 300 analyzed clusters as well as their temporal behavior are provided in the data repository and their assignment to general classes is documented by Table S1.

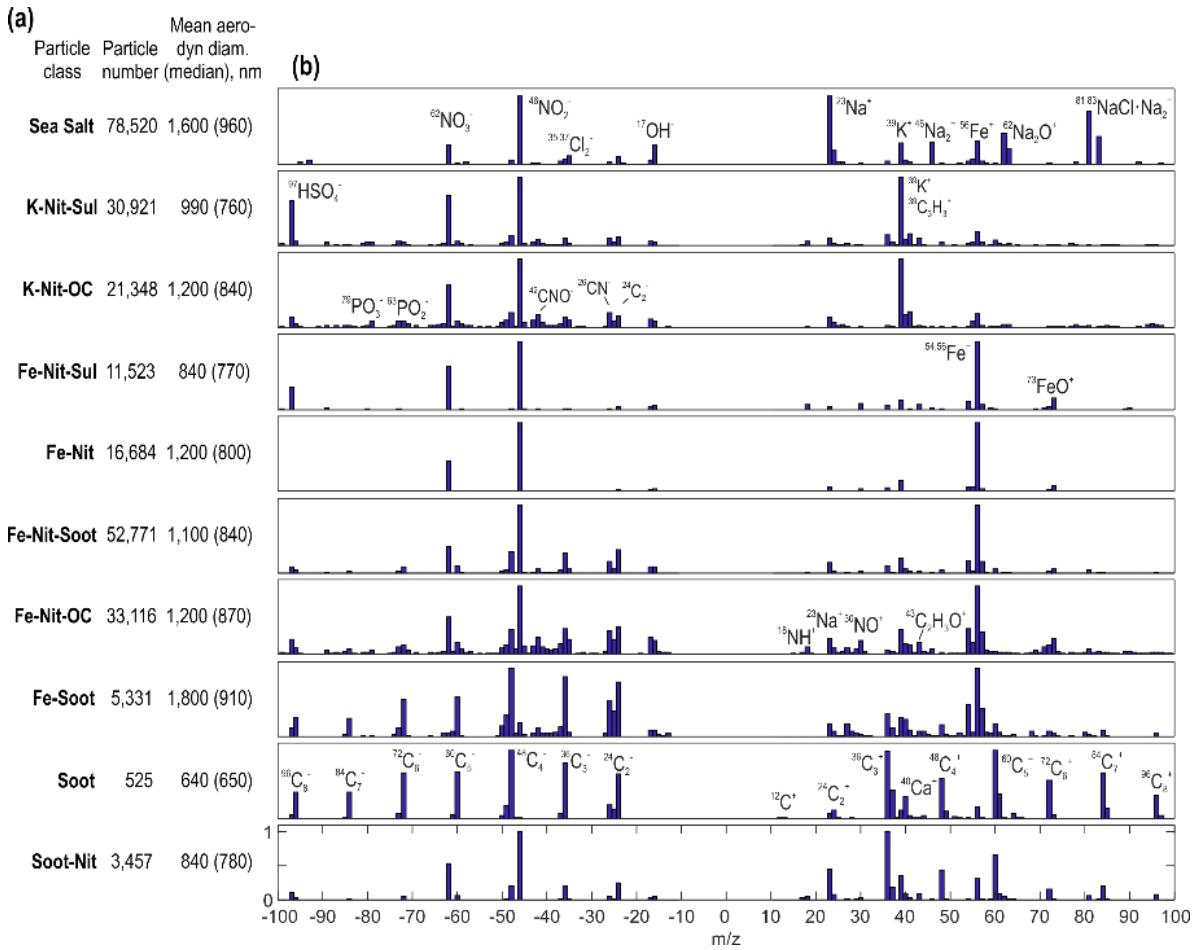

Figure 2(a) Main particle classes obtained from ART-2a clustering of LDI mass spectra, their particle numbers, and size. (b) Weight matrices (spectra of the cluster center) of negative ions (left) and positive ions (right) corresponding to average mass spectra from LDI. Note that iron is resonantly ionized and therefore efficiently detected. The top 300 ART-2a clusters that were manually merged to these classes can be downloaded from the data repository.

The LDI cluster analysis reveals that the aerosol ensemble is dominated by sea salt and by mixtures of carbonaceous particles with nitrate and sulfate. The spectra reveal a relatively high degree of internal mixing (Riemer et al., 2019) compared to SPMS studies in urban regions (Dall'Osto and Harrison, 2006; Healy et al., 2012; Zhang et al., 2013; Giorio et al., 2015; Ma et al., 2016) or marine environments (Middlebrook et al., 1998; Sullivan et al., 2007; Arndt et al., 2017). The strong mixing can be associated with the low contribution of individual local sources, by the geographical location between marine and terrestrial environments with agriculture, forests, and distant urban areas as well as by high wind speeds that enhances long-range

transport. A further reason is the sampling bias towards larger particles with high amounts of secondary material. In the following, the main particle classes are briefly discussed:

Sea salt particles are relatively large and show characteristic signatures from sodium ions (e.g. $^{23}Na^+$, $^{46}Na_2^+$, $^{62}Na_2O^+$, $^{63}Na_2OH^+$), $^{39}K^+$, $^{17}OH^-$ and $^{35,37}Cl^-$ (Dall'Osto et al., 2004; Murphy et al., 2019). To keep the number of classes small, we merged pure sea salt (>50% during high local wind speed), aged sea salt (dominant at calm weather periods), and mixtures of sea salt with carbonaceous particles into this class, as long as the salt signatures were dominating and the characteristic signal of $^{81,83}Na_2Cl^+$ was clearly recognizable.

Particles with a dominating K^+ peak in positive mode are commonly attributed to biomass burning and wood combustion (Silva et al., 1999; Zhang et al., 2013). CN^- and CNO^- peaks in the anion mass spectra were associated with nitrogen-containing organic compounds (Silva and Prather, 2000; Köllner et al., 2017). Here we distinguish between K-Nit particles with strong sulfate signals from the ones showing larger contributions from organic fragments.

Numerous clusters exhibit strong Fe peaks. Of note, we used a KrF-excimer laser with a wavelength of 248.3 nm, thus the photon energy matches a strong absorption line of atomic iron. As a consequence, iron is detected more universally and with much higher sensitivity than in most other SPMS studies (Passig et al., 2020). Mineral dust (Marsden et al., 2018) was not observed, probably because the region is dominated by marine environments and forests in a wide radius. Thus, the iron most likely stems from anthropogenic sources such as coal combustion and engine emissions. The iron bound in soot nanoparticles can enter larger size modes by agglomeration and condensation of secondary material. Most of the clusters with high Fe signals reveal strong peaks of secondary nitrate, indicating distant sources (Furutani et al., 2011; Dall'Osto et al., 2016b). Similar to the K-Nit particles, we found Fe-Nit particles with and without sulfate signature. We also distinguish between particles according to their EC/OC balance (Ferge et al., 2006; Spencer and Prather, 2006), however, this ratio is a continuum in our study (Zhou et al., 2006).

Larger soot agglomerates were mixed with iron and nitrate, but there was also a limited number of relatively fresh soot particles. They showed Ca^+ peaks larger than the K^+ (and fragment) signals at m/z=39. It was shown that the majority of soot particles from engines in the accumulation mode reveal Ca^+ signatures from lubrication oil additives (Sakurai et al., 2003; Sodeman et al., 2005; Toner et al., 2006).

As our study focuses on PAHs and long-range transported combustion aerosols, our LDI-based classification separates into fewer particle types compared to recent studies in Europe (Schmidt et al., 2017; Lacher et al., 2021). Also the limited timeframe of our study and the comparable remote environment with little industrial contribution limit the number of different particle types. The size distribution of all particle classes is shown in Supplemental Figure S1.

3.2 Time series of main particle classes and air mass history

The measurement period was characterized by changing weather conditions with high wind speeds, frequent rain showers, and temperatures varying between 0 °C and 12 °C, during the beginning of the heating season. $PM_{2.5}$ data was available between the 14th and 21tst of October with a mean value of 6.5 µg/m^3, measured with the optical particle counter of the monitoring

station. Fig. 3(a) shows the regions the air masses passed within the last 24h before arriving at the sampling site, as obtained from analysis of the HYSPLIT back trajectories shown in Supplemental Fig. S2. Local wind data from the nearby meteorological station Nidingen is plotted in Fig. 3(b). Particle numbers of the main particle classes with 10 min resolution are shown in Fig. 3(c), while Fig. 3(d) shows the same data normalized to total particle counts without corrections for particle detection efficiencies as performed by (Shen et al., 2018) and (Shen et al., 2019a).

During western wind directions, marine air is transported from the North Sea via Denmark and the Kattegat, thus the aerosol is dominated by sea salt particles. As apparent from Fig. 3(d) Fe-containing particles with soot are more abundant than particles that belong to the K^+-dominated clusters. In addition to remote sources, also marine traffic may contribute. Both the North Sea and the Baltic Sea are Sulphur Emission Control Areas (SECA), where the large majority of ships run on distillate fuels instead of bunker fuels (Lähteenmäki-Uutela et al., 2019). Consequently, particles with signatures of V and Ni were sparsely detected and are therefore not shown separately from Fe-soot mixtures (Moldanová et al., 2009; Healy et al., 2009; Ault et al., 2010; Passig et al., 2021). Despite the marine origin, only a few particles with dominant sulfate signals in anion spectra were detected (Dall'Osto et al., 2016a; Arndt et al., 2017; Wang et al., 2019). Possible reasons comprise the sulfur limits for ship fuels and low marine biogenic activity in autumn.

The highest total particle numbers and smallest contributions from sea salt were observed during eastern winds with air transport from Eastern Europe via the central Baltic Sea and Sweden (16th October). Of note, also the sulfur-containing particles (yellow and cyan) are most abundant during this period, while mixtures with only nitrate dominate outside this period. The sulfur may stem from coal combustion (Xu et al., 2018), which is much more common for residential heating in Eastern Europe than for Western Europe and Scandinavia. K-Nit-Sul particles are the dominating class, reflecting the importance of residential wood combustion in Eastern Europe and Sweden.

The 19th and 20th of October were characterized by air transport from Central Europe via the Southern/Western Baltic Sea. Besides sea salt, iron-containing particles with signatures from nitrate, organics, and soot were most abundant, which can be associated with traffic emissions in densely populated European regions (Dall'Osto et al., 2016a) and warmer temperatures in early autumn, where the heating season has not yet begun. Sulfate is now predominantly detected on iron-containing particles, whereas it was more often associated with potassium-dominated particles during transport from Eastern Europe.

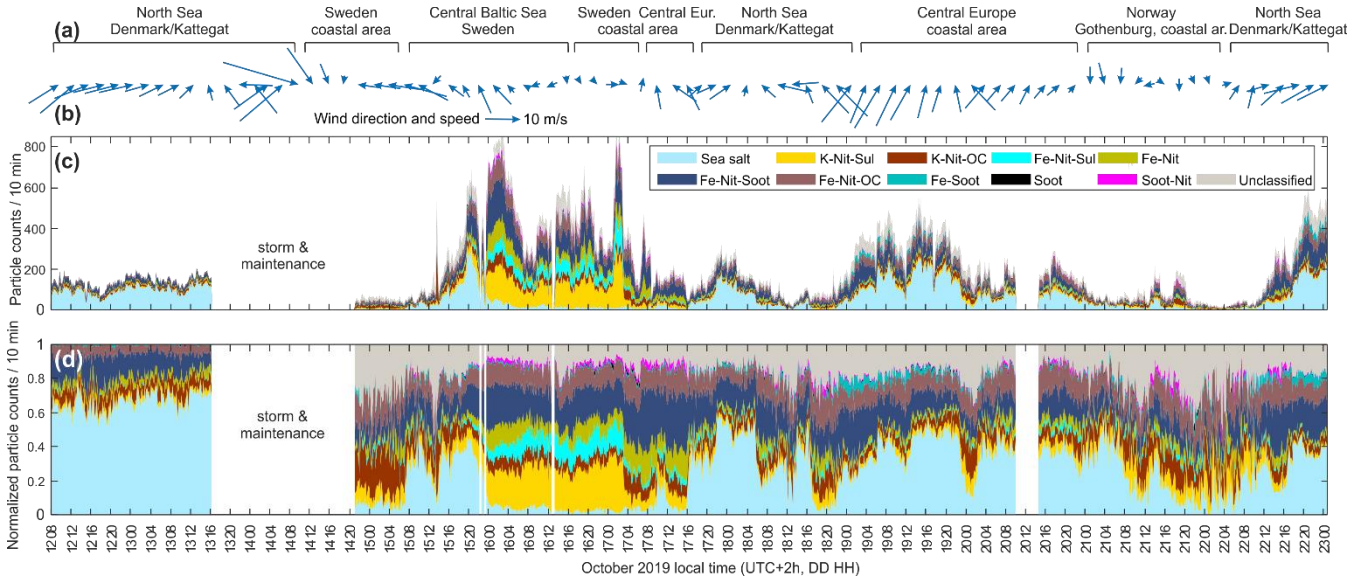

Figure 3: (a) Air mass origin obtained from analysis of the HYSPLIT back trajectories shown in Fig. S2 (top line: >12 h, bottom line <12 h). (b) Local wind data from a meteorological station 8 km south of the measurement site. (c) Time series of particle counts reveal stable conditions with dominating sea salt during strong wind from the sea and higher particle numbers as well as transient features, e.g. from possible night-time particle formation events at light winds from land and along the coastline. (d) The same data as (c), normalized to total particle counts reveals the relative contributions of each particle class. High numbers of sulfate-containing, potassium-rich particles can be noticed during air mass transport from Eastern Europe, where the heating season has already started and wood, as well as coal combustion, is common. Wind from Central Europe transports mainly internal mixtures of Fe, organics, and nitrate. Soot signatures are recognized in many particles, but rather pure soot particles and Fe-soot mixtures without secondary material are limited to south-western on-shore winds, pointing to contributions from marine traffic.

Transient increases in particle numbers can be noticed during low wind speeds on the 16th and 17th of October. Some of them occur at night time, possibly from particle growth into accumulation mode by condensation of secondary material. However, there are also other events such as a green waste burning fire in some kilometers distance in the afternoon of the 15th October and further particle number increases of unknown origin, observed during light wind along the coastline, e.g. on the 17th of October. Within the first period of marine air and strong wind (12th -13th of October), no transient changes in particle numbers and composition were recognized.

While soot signatures appear in many particles with strong Fe-and nitrate signals during the complete measurement period, the Fe-soot particles without nitrate, as well as fresh soot particles, were only observed during southwestern winds. Assuming that nitrate is mainly secondary from terrestrial emissions, these relative fresh soot particles could be associated with marine traffic from the major shipping lanes in southwestern direction.

3.3 REMPI-PAH signatures in particles classified via LDI

3.3.1 General aspects and limitations

Firstly, it should be remembered here, that the peak area in SPMS is not directly convertible to the concentration of a specific substance (Murphy, 2007; Hinz and Spengler, 2007; Reinard and Johnston, 2008; Pratt and Prather, 2012; Healy et al., 2013;

Hatch et al., 2014; Zhou et al., 2016; Gemayel et al., 2017; Shen et al., 2019a). Two-step techniques with separated desorption and ionization, as utilized for the PAHs here, have been shown to be favorable for quantification approaches compared to conventional single-particle LDI (Woods et al., 2001). However, ambiguity remains from different REMPI cross-sections among the PAHs and isomeric structures (Wilkerson et al., 1989; Gehm et al., 2018). Diagnostic ratios for pairs of individual species are typically available for isomeric PAHs (Ravindra et al., 2008; Tobiszewski and Namieśnik, 2012) and are not directly applicable here. The REMPI cross-sections of degradation products and heterocyclic compounds, such as the health-relevant nitro-PAHs, are typically much lower due to distortion of the π-electron system (Zimmermann and Hanley, 2020) and can therefore not be detected on a single-particle level.

3.3.2 Abundance of PAHs in particles classified by LDI mass spectra

Before analyzing the different PAH patterns found across the particle ensemble, we discuss the abundance and distribution of PAHs in the main particle classes from LDI. Similar to Fig. 2, the LDI particle classes are again summarized in Fig. 4(a), with an additional column showing the number of PAH-containing particles as determined by the presence of at least four peaks on the m/z channels 178, 189 (fragment of alkylated phenanthrenes), 202, 220, 228 and 252. Fig. 4(b) depicts the corresponding mean mass spectra of PAHs. A first look reveals that sea salt dominated particles show no PAHs, even though this class contains also aged salt particles with secondary nitrate and very low signals of carbonaceous components, compare LDI mean mass spectra in Fig. 2(b). Harrison et al. found that PAHs from road traffic can be absorbed by salt particles from salting of the road (Harrison et al., 1996). However, for the sea salt particles here, it can be assumed that PAHs were either degraded or in the particulate phase before entering the marine boundary layer and coagulation with sea salt might not be important enough here to detect such mixtures. Also for iron-containing particles with nitrate and/or sulfate, PAH signatures are absent. A general trend becomes already visible here: The stronger the signals of nitrate and sulfate, the lower is the abundance of PAHs in the particles. There is a number of possible explanations. Firstly, thick coatings of secondary material probably reduce the efficiency of laser desorption for the PAH-containing organic matter (Hatch et al., 2014). On the other hand, it was shown that organic layers can protect PAHs also from photochemical degradation (Zelenyuk et al., 2012; Keyte et al., 2013; Shrivastava et al., 2017; Alpert et al., 2021), while the effect of secondary nitrate and sulfate on PAH degradation is less investigated. Secondly, high amounts of secondary species suggest a substantial age of the particles, and thus, PAHs may already have been degraded before. Thirdly, the ionization technique itself may contribute to this trend: Particles that are fully hit by the desorption laser produce more intense PAH spectra via REMPI of the plume. However, secondary nitrate or sulfate is also desorbed to a larger extent from these particles, and less amount of this material remains on the particle for detection via LDI in the second laser shot. Nevertheless, in so-far unpublished field experiments with the same setup during winter in Central Europe, we often found PAHs on more than 20% of all particles, also if strong nitrate- and sulfate signals were present, thus the instrumental aspect seems to be of minor importance here.

As might be expected, particles with OC fragments in LDI spectra also show PAH signatures in REMPI spectra more frequently, see also the relative numbers of PAH-containing particles within the particle classes in Fig. 4(c). However, the

highest PAH abundances can be noticed for soot particles, especially for the relatively fresh and comparably small soot particles. In contrast, the Soot-Nit class shows nearly no PAHs. In addition to some possible effects of the ionization technique, the PAHs might have been degraded from these aged particles or shielded by thick coatings, as mentioned before. Of note, the classes discussed so far account for only 37% of all particles with PAH signatures. 42% of the PAH-containing particles were not within the top-300 clusters from LDI but have at least 4 LDI peaks, mostly from secondary nitrate, K^+, Fe^+, and organic fragments, as revealed by a rough screening. About 21% of the PAH-containing particles show less than four LDI peaks. They were not sufficiently hit by the back-reflected LDI laser beam, because numerous organic fragments and K^+ would otherwise appear in the LDI spectrum.

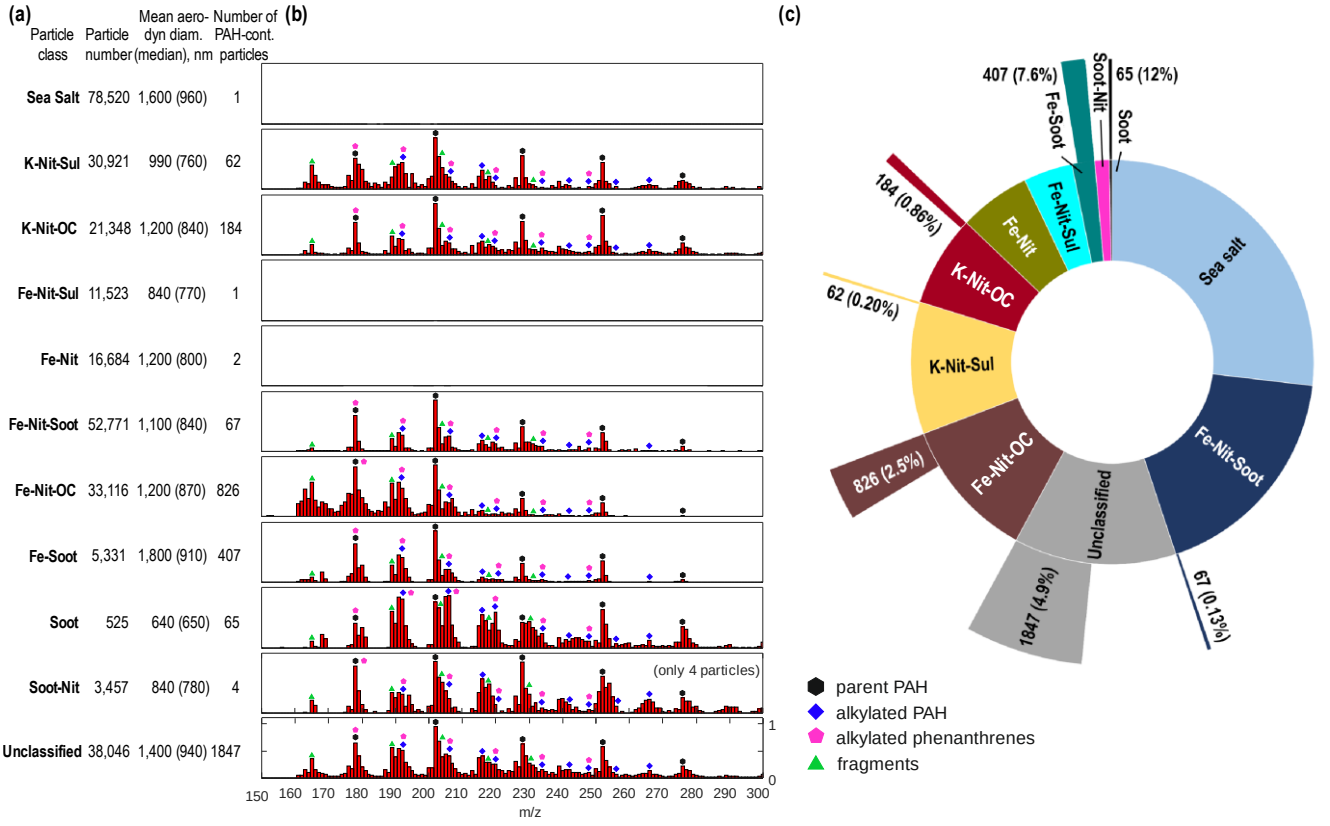

Figure 4: (a) Main particle classes obtained from ART-2a clustering of LDI mass spectra, their particle numbers, size, and the number of PAH-containing particles in the respective class. Sea salt particles and mixtures with strong secondary nitrate and sulfate show rarely PAHs. (b) Averaged REMPI mass spectra of the respective LDI-clusters. Particles with dominating potassium signatures reveal strong signals of high-mass PAHs, e.g. from wood combustion while particles with prominent Fe-signatures show more alkylated and smaller PAHs, as typical for diesel emissions (Zhang et al., 2008; Tobiszewski and Namieśnik, 2012). Fresh soot particles have higher signals of alkylated phenanthrenes. The unclassified particles were not within the top-300 ART-2a clusters but reveal variable LDI signatures, mostly from organic fragments. Particles with less than four peaks in LDI spectra are not shown here, explaining the missing PAH-containing particles. (c) The inner ring of the sunburst plot illustrates the relative abundance of

each LDI-determined particle class. The outer ring depicts the absolute number and number fraction of PAH-containing particles in the respective class. The areas of the outer ring are 10-fold enlarged to make small fractions of PAH-containing particles visible.

3.3.3. Mean PAH signatures in particles classified by LDI mass spectra

When comparing mass spectral patterns of particle-bound PAHs, several aspects beyond the actual experimental details have to be considered. Previous SPMS studies with LD-REMPI ionization (without information on refractory and inorganic components) on fresh emissions have identified source-specific signatures in the mass spectra (Morrical et al., 1998; Bente et al., 2006; Bente et al., 2008, 2009; Li et al., 2019). However, within a multitude of photolysis and oxidation pathways during atmospheric transport, the different PAHs are degraded with different decay rates (Tobiszewski and Namieśnik, 2012; Keyte et al., 2013; Pöschl and Shiraiwa, 2015). Therefore, the PAH distributions observed in studies on long-range transported particles can be substantially different from the patterns observed at a specific source and atmospheric conditions have to be considered (Tobiszewski and Namieśnik, 2012; Nguyen et al., 2021). The degradation mechanisms are complex and interfering, however, as a general trend, alkylated PAHs and light-weight species are often reported to be removed more rapidly (Phousongphouang and Arey, 2002; Lima et al., 2005; Keyte et al., 2013), and differences in the mass-spectral pattern can be expected to be blurred by degradation processes during long-range transport, diminishing source-specific signatures.

As apparent from Fig. 4(b), unsubstituted 'parent' PAHs contribute the most intense PAH peaks for the LDI-based particle classes, with a maximum for pyrene/fluoranthene (m/z=202), see Table 1. Technical problems were resulting in small inaccuracies of the mass spectrometer and slight broadening of high-mass peaks, however, all key features of the mass spectra remained visible. For the K-Nit-Sul particles and the K-Nit-OC class, the peaks at m/z=228 and m/z=252 from parent high-molecular-weight PAHs are the second highest and third highest signals. Such distributions are known for pyrogenic PAHs from wood and coal combustion (Czech et al., 2018), in agreement with the source information from LDI. Also gasoline engines emit unsubstituted PAHs of high molecular weight (Miersch et al., 2019), however, particles from engine emissions have a different inorganic composition (Sodeman et al., 2005; Toner et al., 2006; Toner et al., 2008). The PAH spectra of the K-Nit-Sul and the K-Nit-OC class are almost similar. As mentioned before, K-Nit-OC particles reveal PAH signatures more often, in line with the more pronounced OC fragments in LDI spectra.

Particles with prominent Fe signatures reveal a slightly different mean PAH profile. The PAHs of high molecular weight are less prominent while smaller and alkylated species (e.g. m/z=192 and 206) show a bit more intense peaks, indicative for petrogenic PAHs, e.g. from incomplete combustion in engines (Spencer et al., 2006; Tobiszewski and Namieśnik, 2012; Streibel et al., 2017; Czech et al., 2017). A comparable trend is also documented for PAHs from diesel engines (Spencer et al., 2006). The larger fraction of Fe-containing particles during periods of air mass transport from Central Europe (see Fig. 3) is in accordance with the assumption of higher importance of traffic emissions while wood and coal combustion particles were dominant during wind from Eastern Europe.

The relatively fresh soot particles show a different PAH signature with stronger contributions from alkylated phenanthrenes (e.g. m/z=192, 206, 220, 234). With this pattern, they more resemble diesel engine emissions, e.g. from unburned fuel, than

335 the aged soot particles with nitrate and iron contributions (Spencer et al., 2006; Toner et al., 2006). Most of these particles were detected during on-shore wind, hence ship traffic is the most likely source. The fewer particles observed at eastern wind may stem from local wood combustion and land-based traffic. The PAH signatures of these sources are averaged in the depicted mean spectrum.

A substantial fraction of PAH-containing particles is not classified concerning their inorganic composition because they either
340 produced now LDI mass spectra (21%) or belong to clusters with small particle numbers and high orders beyond 300 (42%), see the bottom row in Fig. 4(b). Their mean PAH spectrum results from different particle types and possible differences between PAH spectra are averaged, emphasizing the need for a single-particle analysis of the PAH spectra.

345

Table 1: Polycyclic aromatic hydrocarbons, indicated by the REMPI mass spectra (m/z).

PAHs	**number of C in aliphatic side chain(s)**				
	0	**1**	**2**	**3**	**4**
naphthalene	128	142	156	170	184
acenaphthene	152				
phenanthrene, anthracene*	178	192	206	220	234
pyrene, fluoranthene	202	216**	230***	244****	
Chrysene, benzoanthracene, benzophenanthrene(s), triphenylene	228	242			
benzopyrene(s), benzofluoranthene(s), perylene	252	266			
benzo[g,h,i]perylene, indeno(1,2,3)[c,d]pyrene	276				
dibenzophenanthrene(s), dibenzoanthracene(s), benzochrysene, picene	278				
important fragments	115, 139, 165, 189				

* alkylated species predominantly belong to the homologuous series of alkylated phenanthrenes

350 ** possible interference with benzofluorenes and cyclopentaphenanthrenes

*** possible interference with terphenyl

**** possible interference with benzylbiphenyl

3.4 Single-particle analysis of PAHs

In the previous analyses, the individual PAH spectra were merged within LDI particle classes that represent their inorganic composition, yielding rather subtle differences among the mean PAH spectra in Fig. 4(b).

To unravel the single-particle PAH composition of the ensemble, we performed a further ART-2a analysis exclusively for the PAH spectra from REMPI. The analysis with a vigilance factor of 0.7 yielded 733 clusters, whereof the top 300 were manually inspected, see the data repository for all 300 cluster spectra. High-mass inorganic compounds such as lead or potassium phosphates also appear in the respective m/z range but can be easily excluded from the PAH analysis by their clearly different signatures. The top 300 clusters include 3746 (84.9%) of in total 4412 PAH-containing particles. The 300 clusters were then manually merged to 10 PAH classes with respect to their main mass spectral characteristics, see Table 2.

Table 2: Main particle classes obtained from ART-2a clustering of PAH mass spectra, their particle numbers, and size. HMW: high molecular weight (four rings or more), LMW: low molecular weight (less than four rings), parent: unsubstituted parent PAHs, OC: organic aside from PAHs. For all cluster spectra see data repository and Supplemental Table S2.

PAH class	'common'	'PAH-HMW'	'parent'	'parent-HMW'	'PAH-OC-LMW'	'PAH-OC-HMW'	'OC-HMW'	'alkylated'	'alkylated-LMW'	'fragmented'
Particle number	1413	161	251	225	650	87	176	168	71	544
Median aerodynamic diameter (nm)	669	558	644	573	872	656	942	369	525	630
Figure	5	6	S3	S4	7	8	S5	9	S6	S7
Context source/process	Highest abundance, strong mixing	Biomass burning	PAH degradation	PAH degradation	Secondary organic	Aged POA/ Oligomerization	Aged POA/ Oligomerization	Ship traffic	Local green waste burning	unknown

In the following, we discuss the most important PAH particle classes and approach the full depth of single-particle information to identify signatures of sources and atmospheric processing in the particle ensemble.

Fig. 5 (a) shows the mass spectrum of the most abundant PAH profile (n=1,413 particles), hereinafter referred to as the 'common' cluster. It is dominated by unsubstituted ('parent') PAHs and peaks for m/z=202. Also, the aforementioned fragment at m/z=189 and smaller signatures of alkylated PAHs (e.g. m/z=206) can be noticed. The averaged LDI spectra from the respective particles (Fig. 5(b)) show strong contributions from EC, K^+, Ca^+, Fe^+, smaller OC peaks, and minor nitrate signals. In Fig. 5(c), all 3,746 PAH-classified particles are shown as grey dots, positioned with respect to their detection time (x-axis) and vacuum aerodynamic diameter (y-axis). The red dots represent the particles of the actual cluster and reveal that particles of the 'common' type appeared during all periods of the measurement, however with increased abundances on November $15^{th}/16^{th}$ during air transport from Eastern Europe, compare Fig. 3.

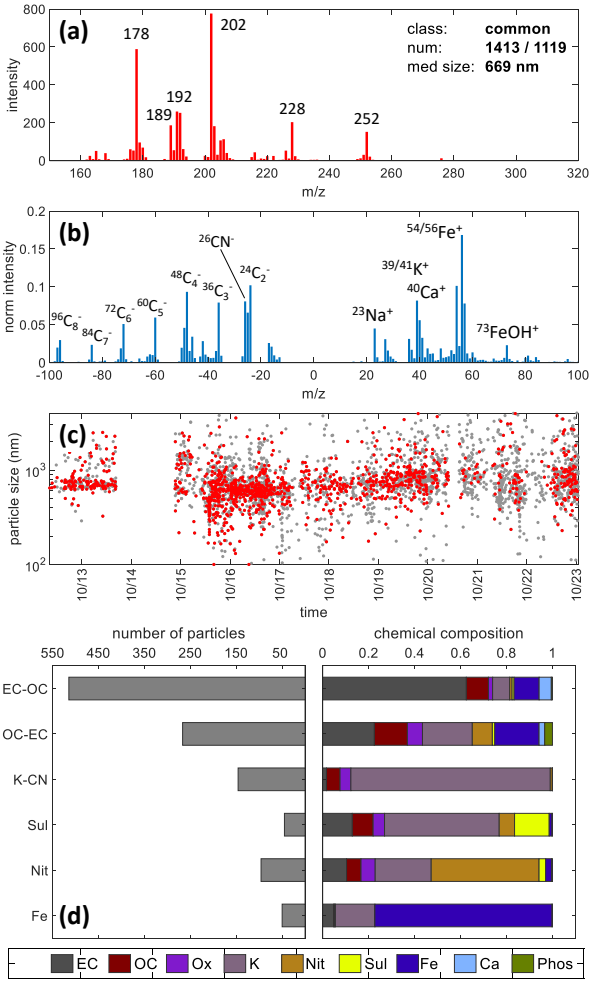

Figure 5: (a) Weight matrix (spectrum of the cluster center) of the most abundant 'common' PAH class (1,413 particles, whereof 1,119 show additional LDI mass spectra with at least four peaks, med size: median vacuum aerodynamic diameter). (b) Averaged LDI mass spectra of the particles that belong to this cluster. (c) Occurrence of these particles (red dots, n=1,413) within the measurement period (x-axis) and their vacuum aerodynamic diameter (y-axis). Grey dots: PAH-containing particles from the other PAH classes 2–10 (n=2,333). (d) Left panel: number of particles in the subgroups as a result of sub-clustering the LDI signatures of particles in the 'common' PAH class. Here, the EC-OC particle type dominates. Right panel: averaged relative peak areas of the key inorganic components for the particles in the subgroups. Ion mass channels: EC: 24–84/36, 48; OC: 42/27, 29, 55, 63; Ox: 45, 59, 71/43 (oxygen-containing fragments); K: -/39; Nit: 46, 62/-; Sul: 97, 99/-; Fe: -/54, 56; Ca: -/40; Phos: 63, 79/- for negative/positive m/z, respectively.

To untangle the interrelations between PAHs, the particles' inorganic composition, and atmospheric processing, we performed a sub-analysis of the particles' inorganic composition for the 10 PAH types. This sub-clustering of LDI signals from the particles of each PAH-class was performed with a vigilance factor of 0.7 and the results were manually merged to six subgroups, each representing the key characteristics of the particle composition from LDI . The result for the 'common' PAH-particle type is depicted in Fig. 5(d). The left panel shows the number of particles in each subgroup and the right panel the averaged inorganic composition of the particles in the respective subgroup. For example, this allows comparing the chemical composition of the EC-OC subgroup of particles belonging to one of the PAH classes to the respective EC-OC subgroup of another one of the 10 PAH classes.

It is impossible to discuss all details in this unprecedented dataset, so we focus on our most important findings and refer to the Supplemental Figs. S3–S7, where corresponding plots for further PAH classes can be found.

The majority of particles with a 'common' PAH profile show dominant EC signatures (Fig. 5(d)), while also all other particle subgroups occur. Both Fe^+ (traffic, industrial) and K^+ (if dominant: biomass burning) signatures can be recognized among most particle subgroups, indicating that this PAH pattern is not indicative for some specific source but rather a result from extended mixing and atmospheric processing. This is in line with the typical size of the particles (Fig. 5(c)) well above common sizes of fresh soot emissions and with the ubiquitous occurrence during the entire measurement period; both speak against local sources.

3.4.2 Traffic and biomass burning source profiles

The PAH-HMW cluster shown in Fig. 6 is characterized by a peak pattern that extends to much higher masses compared to the 'common' class in Fig. 5. Such particles were occasionally detected during the full measurement period, with increased numbers in the evening of November 19th and 21st. The mean LDI spectra (Fig. 6(b)) and the single-particle inorganic composition (Fig. 6(d)) reveal that EC-particles are the most abundant group showing this PAH profile and OC fragment signals are rather small. In contrast to the 'common' PAH class in Fig. 5, the positive mass spectra are dominated by the K^+ peak, while Fe^+ is virtually absent, pointing on wood/biomass burning sources (Lee et al., 2016; Dall'Osto et al., 2016a).

High ratios of HMW/LMW-PAHs have been discussed as an indicator for both fossil fuels and wood combustion (Zhang et al., 2008; Ravindra et al., 2008; Tobiszewski and Namieśnik, 2012). For the long-range transported particles in our study, strong signals of HMW PAHs are consistently associated with wood/biomass signatures from LDI. Both the volatilization of LMW PAHs and their rapid degradation in the gas phase (Lima et al., 2005; Keyte et al., 2013) as well as possible shielding effects from internal mixing with low-volatility biomass burning organic aerosol (Shrivastava et al., 2017; Alpert et al., 2021) can be assumed to play an important role here. In conventional LDI-based source apportionment in SPMS, biomass burning particles are typically identified by their K^+ and CN^- peaks (Dall'Osto et al., 2016a). An important finding here is that additional PAH information can help to identify the EC particles from biomass combustion. Coal combustion may contribute a comparable PAH pattern (Xu et al., 2018) but because of the absence of peaks from Fe and other transition metals, it is an unlikely source here.

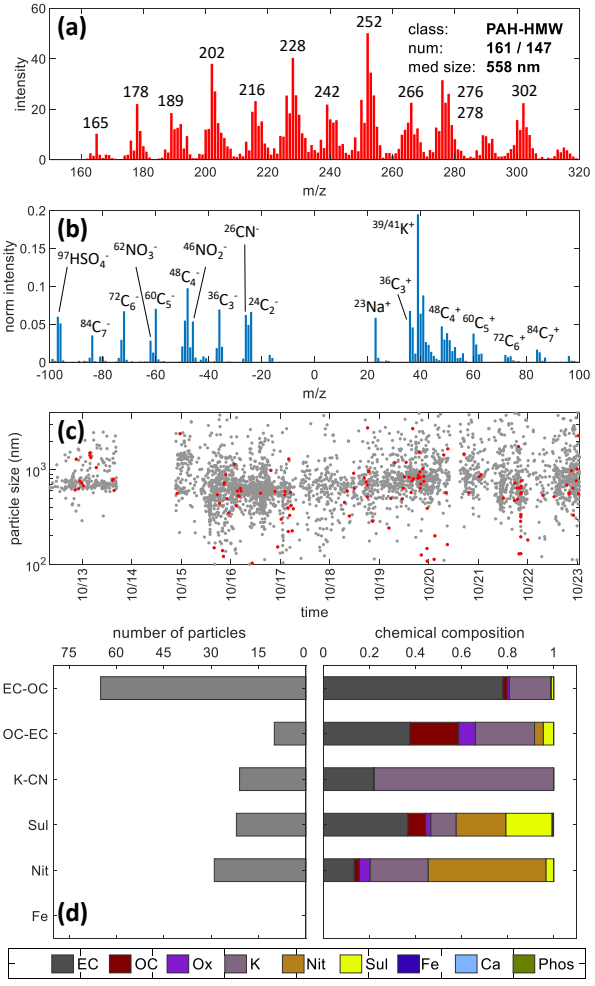

Figure 6: PAH patterns up to high molecular weights are associated with strong K^+ signals and the absence of Fe^+, giving evidence for biomass burning particles. (For figure explanation, see Fig. 5.)

3.4.3 PAH degradation

Two PAH clusters reveal only the parent PAHs, while further peaks from fragments and substitutes are absent, see Supplemental Figs. S3 and S4. The inorganic composition of particles from the 'parent' PAH cluster shown in Fig. S3 resembles the 'common' cluster (Fig. 5), however with increased contributions from nitrate. The nitrate signatures of secondary

material are further enhanced for the 'parent' PAH cluster with high molecular weight PAHs (Fig. S4). The shift towards high-mass PAHs can again be associated with the biomass burning contribution by the absence of Fe and the dominance of K in the particle's inorganic composition. However, in direct comparison to the 'HMW' PAH cluster in Fig. 6, the particles in the 'parent HMW' PAH cluster in Fig. S4 show more frequently strong signals of secondary nitrate and sulfate. Thus, the observation of peaks from solely unsubstituted PAHs may indicate PAH degradation, as the alkylated PAHs tend to have shorter half-lives (Garrett et al., 1998; Lima et al., 2005) and some of the larger PAHs are more stable against photo-oxidation processes in the particulate phase (Keyte et al., 2013). PAH degradation in airborne particles is strongly affected by matrix effects and varying atmospheric conditions. Laboratory experiments can hardly represent the matrix of organic and inorganic secondary material and possible shielding effects (Zelenyuk et al., 2012; Abramson et al., 2013; Shrivastava et al., 2017; Alpert et al., 2021). PAH lifetimes for homogeneous reactions with oxidized N species are reported between 1 hour and 2 days while lifetimes towards heterogeneous photochemical degradation are estimated between few hours and >10 days, both for typical continental background conditions in mid latitudes, see (Keyte et al., 2013) end references therein. Long-range transport of PAHs is well documented, while concentrations measured at remote sites are typically more than one order of magnitude lower than within the respective source regions (Jaward et al., 2004). Evaluation of single-particle PAH signatures may therefore provide a rough estimate on degradation, if the source profile is known or indicated by the inorganic particle composition in a sophisticated future measurement scenario.

3.4.4 Secondary organic material

The REMPI spectra of several PAH classes are characterized by rows of peaks in addition to the PAH signatures. The PAH spectrum in Fig. 7(a) resembles the 'common' type (Fig. 5(a)), however, additional peaks in the low molecular weight range are clearly visible. The average LDI spectra in Fig. 7(b) shows slightly higher fragment signals compared to Fig. 5(b); in particular, the peak at m/z=43 – an established marker for oxygen-containing organic material due to the contribution of $^{43}C_2H_3O^+$ – is increased (Silva and Prather, 2000; Köllner et al., 2017). The particles of this PAH cluster were larger on average and they were more frequently detected in air masses with a terrestrial background compared to marine air (Fig. 7(c)). In conjunction with the high number of nitrate-containing particles in this PAH-cluster (Fig. 7(d)), we assume a high amount of secondary organic material and secondary nitrate for this type of particles (Shen et al., 2019b; Huang et al., 2019).

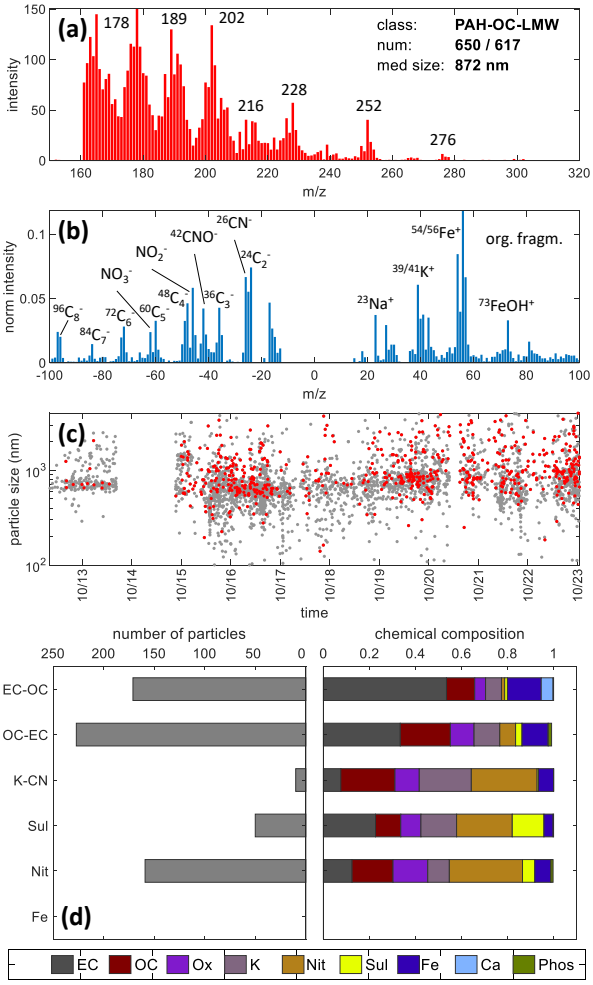

Figure 7: Additional peaks from OC, relatively large particle size, and frequently detected $^{46}NO_2^-$ and $^{62}NO_3^-$ signals indicate the uptake of secondary material. (For figure explanation, see Fig. 5.)

3.4.5 High molecular weight organics and oligomer formation

The PAH-cluster shown in Fig. 8 reveals PAH peaks and organics up to higher molecular weights (PAH-OC-HMW). The inorganic composition differs from the PAH-OC-LMW cluster (Fig. 7) in two major aspects: Firstly, Fe-signatures are smaller and can only be found in some EC-dominated particles. This can explain the HMW-PAHs, which were already associated with biomass burning sources under the conditions of our study (Sec. 3.4.2). Secondly, the particle's secondary composition reveals strong sulfate signals in addition to the nitrate. The HMW-PAH cluster in Fig. 6 shows a comparable distribution of PAHs but fewer other organic signatures and less sulfate, suggesting a link between sulfate and HMW-organics. Accelerated oligomer formation by particle acidity is well established (Gross et al., 2006; Denkenberger et al., 2007; Wang et al., 2010; Riva et al.,

2019), however, also the presence of PAHs itself was found to affect oligomer formation (Zelenyuk et al., 2017; Vereecken, 2018). The small particle number in our experiment allows no statistically sound analysis of the interrelations between these aerosol components, however, more systematic and sophisticated studies based on our approach will provide deeper insights. Of note, oligomerization refers not to the PAHs themselves in our study, as their concentration is probably too low and the resulting signatures would be expected in the mass range beyond m/z=300. Consequently, we assume that non-aromatic oligomers and heterogenic reactions between the PAHs and e.g. OH- contribute to these signatures ('aged primary organic aerosol, POA').

A further cluster with HMW organics and weaker PAH signatures is shown in Fig. S5. The inorganic composition of particles in this OC-HMW cluster shares the high nitrate and sulfate signals of the PAH-OC-HMW cluster in Fig. 8, however, the EC signatures are nearly absent, emphasizing the close connection of PAHs to EC.

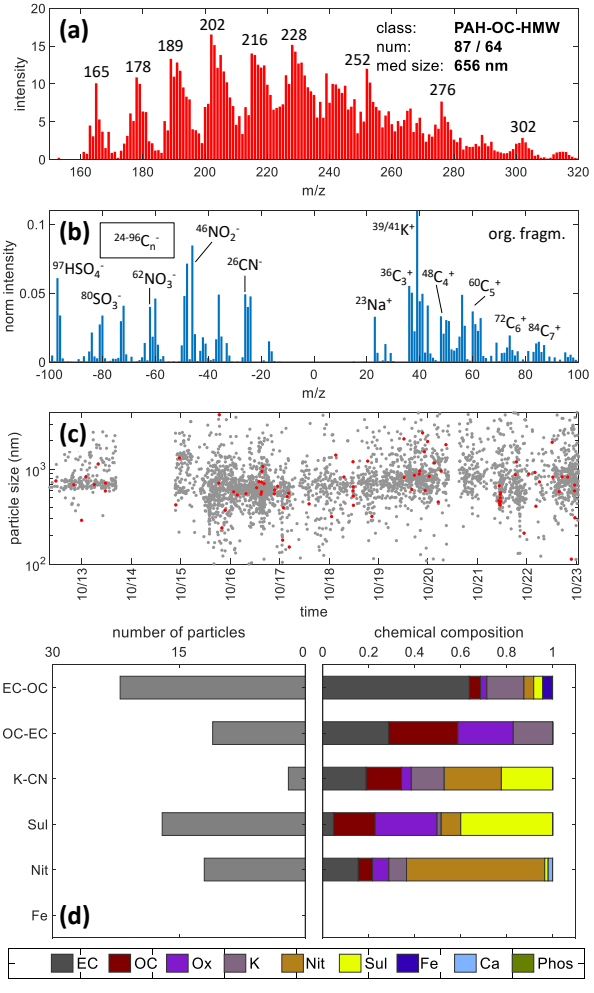

Figure 8: High molecular weight organics in addition to PAH peaks are frequently associated with fragments from oxidized OC (e.g. $^{43}C_2H_3O^+$) and high sulfate signals. This supports the promoted SOA formation and oligomerization in acidic particles. Note also the cluster with dominating HMW-OC and high sulfate signals in Fig. S5. (For figure explanation, see Fig. 5.)

3.4.6 Local sources

In addition to the aged and mixed particles from remote regions, the cluster analysis of PAH spectra revealed also signatures that can be attributed to local sources. The aforementioned green waste burning fire on the 15th of October (see Fig. 3) produced a particle type with solely LMW-PAHs and a high peak of a methylphenanthrene at m/z=192, see Fig. S6. Many of these particles show dominant K^+ peaks that are characteristic for biomass- and wood burning emissions (Silva et al., 1999). Also nitrate and especially sulfate signals are small, as expected for relatively fresh particles.

A unique signature was occasionally observed during onshore wind, with a PAH spectrum that is dominated by alkylated phenanthrenes, see Fig. 9(a). The inorganic composition of these comparable small particles is characterized by strong EC signatures while signals from nitrate and sulfate are rarely detected, indicating rather fresh emissions from a nearby source (Fig. 9b-d). Furthermore, this is the only particle type with strong Ca^+ signals. The combination of EC and Ca indicates combustion engine emissions, which

frequently exhibit Ca^+ signals from lubrication oil additives (Toner et al., 2006). These particles can be associated with marine traffic at the main shipping lane in approximately 30 km distance. The PAH profile with dominant signals from alkylated phenanthrenes that peak around m/z=206 was previously observed in the analysis of volatile to semi-volatile aromatic compounds in ship emissions (Czech et al., 2017). Of note, the entire Baltic Sea is a sulfur emission control area, where conventional high-sulfur bunker fuels are prohibited and most ships are operated with distillate fuels (Lähteenmäki-Uutela et al., 2019). Thus, the characteristic metal and sulfate signals from residual fuels are not observed here (Healy et al., 2009; Ault et al., 2010; Passig et al., 2021).

A further cluster exhibits a characteristic fragmentation pattern with additional peaks at -2 m/z for each PAH signal, see Fig. S7. While this fragmentation pathway is documented for PAHs (Kruth et al., 2017), the correlations of these signatures with the inorganic composition or atmospheric conditions could not be explored so far and will be subject to a future investigation.

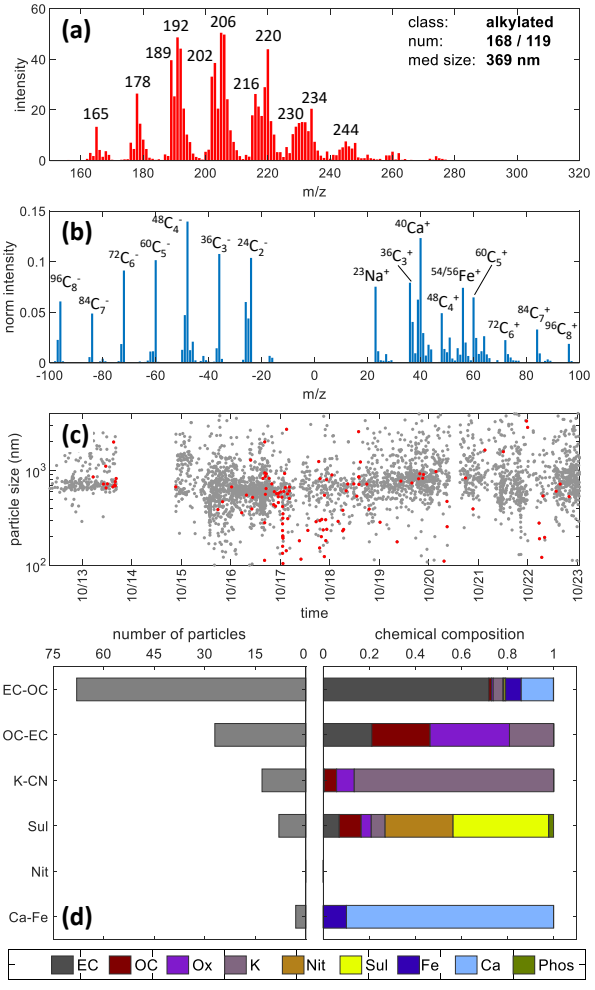

Fig. 9: Particles with dominant signals from alkylated phenanthrenes were observed during onshore wind periods. These rather small particles reveal soot and Ca^+, but nearly no secondary material. They can be attributed to ship traffic with distillate fuels such as marine gas oil. (For figure explanation, see Fig. 5.)

4. Conclusions

In summary, we described the single-particle mass-spectral profiles and distribution of PAHs in ambient air in a rural coastal area in autumn. Therefore, we presented two different approaches to tackle this complex and multi-dimensional dataset. Firstly, we classified the particles concerning their inorganic composition and identified the major carriers of PAHs. We found that the averaged PAH profiles are relatively uniform for most of the particle classes and attributed this to mixing and PAH degradation during atmospheric transport. However, the source-specific inorganic composition of the particles could be linked with pyrogenic and petrogenic PAH signatures. Secondly, we classified the particles with respect to characteristic PAH patterns and provided single-particle information on the inorganic composition of the respective PAH classes. Thereby, a number of distinct PAH profiles could be identified. We associated them with different particle sources

and important atmospheric processes, including PAH degradation, secondary aerosol formation, and oligomerization. Here, a critical step has endeavored as some of these interpretations are provisional because of the limited number of particles, the lack of reference data, and the novel type of data without precedent. Therefore, we desist from extensive correlation analyses and statistics, provide as much insight into the chemical data as possible and try to leave room for interpretation by the reader and an open discussion. Future studies including transport modelling for reliable determination of source regions, quantification approaches and simultaneous operation of established on-line technologies such as the Aerodyne AMS (Canagaratna et al., 2007) are planned, as well as experiments targeting on the PAH distribution in smaller particles, e.g. from local sources and particle formation events, which can hardly be detected with the current setup.

The presented data provide a snapshot of the PAH pollution in a specific region and timeframe, where the conditions were characterized by relatively clean air and dominant long-range transport. However, the study is the first of a series of such measurements that will shed a light on the respective situations in different regions and seasons. While the PAH burden appeared relatively low here, with only about 1.5% of the particles showing clear PAH signatures, we found PAHs on more than 20% of analyzed particles during extended periods of a winter measurement campaign that will be published in a follow-up paper.

Data availability

All cluster mass spectra from the ART2a analyses as well as their time series are available in electronic format from the data repository (https://doi.org/10.5281/zenodo.5794078). All further dataare available on request from Johannes Passig (johannes.passig@uni-rostock.de).

Author contributions

JP and JS contributed equally to this work. JP conceived the study. JS performed the experiments with support from RI, TKB, TA, MS, TS and HF. JS and JP analyzed the data and prepared the figures. HC and RZ provided assistance with data interpretation. JM and HF hosted and supported the field study. JP wrote the manuscript with contributions from all authors.

Competing interests

The authors declare that they have no conflict of interest.

Acknowledgements

We thank Johan Mellqvist, John Conway, Lars Eriksson and co-workers from the Chalmers University of Technology and from the IVL Swedish Environmental Research Institute for hosting the field experiments and their support.

595 The authors gratefully acknowledge the NOAA Air Resources Laboratory (ARL) for the provision of the HYSPLIT transport and dispersion model and READY website (https://www.ready.noaa.gov, last access: 20th August 2021) used in this publication.

Financial support

This research has been supported by the Helmholtz-Gemeinschaft (International Lab aerohealth (Interlabs-0005) and Virtual
600 Institute of Complex Molecular Systems in Environmental Health, HICE), by the Deutsche Forschungsgemeinschaft (grant no. ZI 764/6-1) and the Bundesministerium für Wirtschaft und Energie (grant no. ZF4402101ZG7 and 16KN083626).

References

Abramson, E., Imre, D., Beránek, J., Wilson, J., and Zelenyuk, A.: Experimental determination of chemical diffusion within
605 secondary organic aerosol particles, Physical chemistry chemical physics PCCP, 15, 2983–2991, https://doi.org/10.1039/c2cp44013j, 2013.

Agudelo-Castañeda, D. M., Teixeira, E. C., Schneider, I. L., Lara, S. R., and Silva, L. F.: Exposure to polycyclic aromatic hydrocarbons in atmospheric PM1.0 of urban environments: Carcinogenic and mutagenic respiratory health risk by age groups, Environmental Pollution, 224, 158–170, https://doi.org/10.1016/j.envpol.2017.01.075, 2017.

610 Alpert, P. A., Dou, J., Corral Arroyo, P., Schneider, F., Xto, J., Luo, B., Peter, T., Huthwelker, T., Borca, C. N., Henzler, K. D., Schaefer, T., Herrmann, H., Raabe, J., Watts, B., Krieger, U. K., and Ammann, M.: Photolytic radical persistence due to anoxia in viscous aerosol particles, Nature Communications, 12, 1769, https://doi.org/10.1038/s41467-021-21913-x, 2021.

Arndt, J., Sciare, J., Mallet, M., Roberts, G. C., Marchand, N., Sartelet, K., Sellegri, K., Dulac, F., Healy, R. M., and
615 Wenger, J. C.: Sources and mixing state of summertime background aerosol in the north-western Mediterranean basin, Atmos. Chem. Phys., 17, 6975–7001, https://doi.org/10.5194/acp-17-6975-2017, 2017.

Ault, A. P., Gaston, C. I., Wang, Y., Dominguez, G., Thiemens, M. H., and Prather, K. A.: Characterization of the single particle mixing state of individual ship plume events measured at the Port of Los Angeles, Environ. Sci. Technol., 44, 1954–1961, https://doi.org/10.1021/es902985h, 2010.

620 Bente, M., Adam, T., Ferge, T., Gallavardin, S., Sklorz, M., Streibel, T., and Zimmermann, R.: An on-line aerosol laser mass spectrometer with three, easily interchangeable laser based ionisation methods for characterisation of inorganic and aromatic compounds on particles, Int. J. Mass Spectrom., 258, 86–94, https://doi.org/10.1016/j.ijms.2006.08.015, 2006.

Bente, M., Sklorz, M., Streibel, T., and Zimmermann, R.: Thermal desorption-multiphoton ionization time-of-flight mass spectrometry of individual aerosol particles: a simplified approach for online single-particle analysis of polycyclic aromatic hydrocarbons and their derivatives, Anal. Chem., 81, 2525–2536, https://doi.org/10.1021/ac802296f, 2009.

Bente, M., Sklorz, M., Streibel, T., and Zimmermann, R.: Online laser desorption-multiphoton postionization mass spectrometry of individual aerosol particles: molecular source indicators for particles emitted from different traffic-related and wood combustion sources, Anal. Chem., 80, 8991–9004, https://doi.org/10.1021/ac801295f, 2008.

Boesl, U.: Laser mass spectrometry for environmental and industrial chemical trace analysis, J. Mass Spectrom., 35, 289–304, https://doi.org/10.1002/(SICI)1096-9888(200003)35:3<289:AID-JMS960>3.0.CO;2-Y, 2000.

Canagaratna, M. R., Jayne, J. T., Jimenez, J. L., Allan, J. D., Alfarra, M. R., Zhang, Q., Onasch, T. B., Drewnick, F., Coe, H., Middlebrook, A., Delia, A., Williams, L. R., Trimborn, A. M., Northway, M. J., DeCarlo, P. F., Kolb, C. E., Davidovits, P., and Worsnop, D. R.: Chemical and microphysical characterization of ambient aerosols with the aerodyne aerosol mass spectrometer, Mass Spectrom. Rev., 26, 185–222, https://doi.org/10.1002/mas.20115, 2007.

Carpenter, G. A., Grossberg, S., and Rosen, D.: ART 2-A: an adaptive resonance algorithm for rapid category learning and recognition, in: IJCNN-91-Seattle International Joint Conference on Neural Networks, 151-156 vol.2, 1991.

Czech, H., Miersch, T., Orasche, J., Abbaszade, G., Sippula, O., Tissari, J., Michalke, B., Schnelle-Kreis, J., Streibel, T., Jokiniemi, J., and Zimmermann, R.: Chemical composition and speciation of particulate organic matter from modern residential small-scale wood combustion appliances, Sci. Total Environ., 612, 636–648, https://doi.org/10.1016/j.scitotenv.2017.08.263, 2018.

Czech, H., Stengel, B., Adam, T., Sklorz, M., Streibel, T., and Zimmermann, R.: A chemometric investigation of aromatic emission profiles from a marine engine in comparison with residential wood combustion and road traffic: Implications for source apportionment inside and outside sulphur emission control areas, Atmospheric Environ., 167, 212–222, https://doi.org/10.1016/j.atmosenv.2017.08.022, 2017.

Dall'Osto, M. and Harrison, R. M.: Chemical characterisation of single airborne particles in Athens (Greece) by ATOFMS, Atmospheric Environ., 40, 7614–7631, https://doi.org/10.1016/j.atmosenv.2006.06.053, 2006.

Dall'Osto, M., Beddows, D. C. S., McGillicuddy, E. J., Esser-Gietl, J. K., Harrison, R. M., and Wenger, J. C.: On the simultaneous deployment of two single particle mass spectrometers at an urban background and a roadside site during SAPUSS, Atmos. Chem. Phys., 16, 9693–9710, https://doi.org/10.5194/acp-16-9693-2016, 2016a.

Dall'Osto, M., Beddows, D. C. S., Harrison, R. M., and Onat, B.: Fine Iron Aerosols Are Internally Mixed with Nitrate in the Urban European Atmosphere, Environ. Sci. Technol., 50, 4212–4220, https://doi.org/10.1021/acs.est.6b01127, 2016b.

Dall'Osto, M., Beddows, D. C. S., Kinnersley, R. P., Harrison, R. M., Donovan, R. J., and Heal, M. R.: Characterization of individual airborne particles by using aerosol time-of-flight mass spectrometry at Mace Head, Ireland, J. Geophys. Res., 109, n/a-n/a, https://doi.org/10.1029/2004JD004747, 2004.

Dat, N.-D. and Chang, M. B.: Review on characteristics of PAHs in atmosphere, anthropogenic sources and control technologies, Science of The Total Environment, 609, 682–693, https://doi.org/10.1016/j.scitotenv.2017.07.204, 2017.

Decesari, S., Allan, J., Plass-Duelmer, C., Williams, B. J., Paglione, M., Facchini, M. C., O'Dowd, C., Harrison, R. M., Gietl, J. K., Coe, H., Giulianelli, L., Gobbi, G. P., Lanconelli, C., Carbone, C., Worsnop, D., Lambe, A. T., Ahern, A. T., Moretti, F., Tagliavini, E., Elste, T., Gilge, S., Zhang, Y., and Dall'Osto, M.: Measurements of the aerosol chemical composition and mixing state in the Po Valley using multiple spectroscopic techniques, Atmos. Chem. Phys., 14, 12109–12132, https://doi.org/10.5194/acp-14-12109-2014, 2014.

Denkenberger, K. A., Moffet, R. C., Holecek, J. C., Rebotier, T. P., and Prather, K. A.: Real-time, single-particle measurements of oligomers in aged ambient aerosol particles, Environ. Sci. Technol., 41, 5439–5446, 2007.

Ferge, T., Karg, E., Schröppel, A., Coffee, K. R., Tobias, H. J., Frank, M., Gard, E. E., and Zimmermann, R.: Fast determination of the relative elemental and organic carbon content of aerosol samples by on-line single-particle aerosol time-of-flight mass spectrometry, Environ. Sci. Technol., 40, 3327–3335, https://doi.org/10.1021/es050799k, 2006.

Furutani, H., Jung, J., Miura, K., Takami, A., Kato, S., Kajii, Y., and Uematsu, M.: Single-particle chemical characterization and source apportionment of iron-containing atmospheric aerosols in Asian outflow, J. Geophys. Res., 116, 5504, https://doi.org/10.1029/2011JD015867, 2011.

Garrett, R., Pickering, I., Haith, C., and Prince, R.: Photooxidation of Crude Oils, Environ. Sci. Technol., 32, 3719–3723, https://doi.org/10.1021/es980201r, 1998.

Gehm, C., Streibel, T., Passig, J., and Zimmermann, R.: Determination of Relative Ionization Cross Sections for Resonance Enhanced Multiphoton Ionization of Polycyclic Aromatic Hydrocarbons, Appl. Sci., 8, https://doi.org/10.3390/app8091617, 2018.

Gemayel, R., Temime-Roussel, B., Hayeck, N., Gandolfo, A., Hellebust, S., Gligorovski, S., and Wortham, H.: Development of an analytical methodology for obtaining quantitative mass concentrations from LAAP-ToF-MS measurements, Talanta, 174, 715–724, https://doi.org/10.1016/j.talanta.2017.06.050, 2017.

Giorio, C., Tapparo, A., Dall'Osto, M., Beddows, D. C. S., Esser-Gietl, J. K., Healy, R. M., and Harrison, R. M.: Local and regional components of aerosol in a heavily trafficked street canyon in central London derived from PMF and cluster analysis of single-particle ATOFMS spectra, Environ. Sci. Technol., 49, 3330–3340, https://doi.org/10.1021/es506249z, 2015.

Gross, D. S., Gälli, M. E., Kalberer, M., Prevot, A. S. H., Dommen, J., Alfarra, M. R., Duplissy, J., Gaeggeler, K., Gascho, A., Metzger, A., and Baltensperger, U.: Real-time measurement of oligomeric species in secondary organic aerosol with the aerosol time-of-flight mass spectrometer, Anal. Chem., 78, 2130–2137, https://doi.org/10.1021/ac060138l, 2006.

Gunzer, F., Krüger, S., and Grotemeyer, J.: Photoionization and photofragmentation in mass spectrometry with visible and UV lasers, Mass Spectrom. Rev., 38, 202–217, https://doi.org/10.1002/mas.21579, 2019.

Hanna, S. J., Campuzano-Jost, P., Simpson, E. A., Robb, D. B., Burak, I., Blades, M. W., Hepburn, J. W., and Bertram, A. K.: A new broadly tunable (7.4–10.2eV) laser based VUV light source and its first application to aerosol mass spectrometry, Int. J. Mass Spectrom., 279, 134–146, https://doi.org/10.1016/j.ijms.2008.10.024, 2009.

690 Harrison, R. M., Smith, D. J. T., and Luhana, L.: Source Apportionment of Atmospheric Polycyclic Aromatic Hydrocarbons Collected from an Urban Location in Birmingham, U.K, Environ. Sci. Technol., 30, 825–832, https://doi.org/10.1021/es950252d, 1996.

Hatch, L. E., Pratt, K. A., Huffman J. Alex, Jimenez, J. L., and Prather, K. A.: Impacts of Aerosol Aging on Laser Desorption/Ionization in Single-Particle Mass Spectrometers, Aerosol Sci. Technol., 48, 1050–1058,
695 https://doi.org/10.1080/02786826.2014.955907, 2014.

Hatch, L. E., Creamean, J. M., Ault, A. P., Surratt, J. D., Chan, M. N., Seinfeld, J. H., Edgerton, E. S., Su, Y., and Prather, K. A.: Measurements of isoprene-derived organosulfates in ambient aerosols by aerosol time-of-flight mass spectrometry - part 1: single particle atmospheric observations in Atlanta, Environ. Sci. Technol., 45, 5105–5111, https://doi.org/10.1021/es103944a, 2011.

700 Healy, R. M., Sciare, J., Poulain, L., Crippa, M., Wiedensohler, A., Prévôt, A. S. H., Baltensperger, U., Sarda-Estève, R., McGuire, M. L., Jeong, C.-H., McGillicuddy, E., O'Connor, I. P., Sodeau, J. R., Evans, G. J., and Wenger, J. C.: Quantitative determination of carbonaceous particle mixing state in Paris using single-particle mass spectrometer and aerosol mass spectrometer measurements, Atmos. Chem. Phys., 13, 9479–9496, https://doi.org/10.5194/acp-13-9479-2013, 2013.

705 Healy, R. M., Sciare, J., Poulain, L., Kamili, K., Merkel, M., Müller, T., Wiedensohler, A., Eckhardt, S., Stohl, A., Sarda-Estève, R., McGillicuddy, E., O'Connor, I. P., Sodeau, J. R., and Wenger, J. C.: Sources and mixing state of size-resolved elemental carbon particles in a European megacity: Paris, Atmos. Chem. Phys., 12, 1681–1700, https://doi.org/10.5194/acp-12-1681-2012, 2012.

Healy, R. M., O'Connor, I. P., Hellebust, S., Allanic, A., Sodeau, J. R., and Wenger, J. C.: Characterisation of single particles
710 from in-port ship emissions, Atmospheric Environ., 43, 6408–6414, https://doi.org/10.1016/j.atmosenv.2009.07.039, 2009.

Hinz, K.-P. and Spengler, B.: Instrumentation, data evaluation and quantification in on-line aerosol mass spectrometry, Journal of mass spectrometry JMS, 42, 843–860, https://doi.org/10.1002/jms.1262, 2007.

Hinz, K.-P., Kaufmann, R., and Spengler, B.: Laser-Induced Mass Analysis of Single Particles in the Airborne State, Anal.
715 Chem., 66, 2071–2076, https://doi.org/10.1021/ac00085a023, 1994.

Huang, W., Saathoff, H., Shen, X., Ramisetty, R., Leisner, T., and Mohr, C.: Chemical Characterization of Highly Functionalized Organonitrates Contributing to Night-Time Organic Aerosol Mass Loadings and Particle Growth, Environ. Sci. Technol., 53, 1165–1174, https://doi.org/10.1021/acs.est.8b05826, 2019.

Jaward, F. M., Farrar, N. J., Harner, T., Sweetman, A. J., and Jones, K. C.: Passive air sampling of polycyclic aromatic
720 hydrocarbons and polychlorinated naphthalenes across Europe, Environmental toxicology and chemistry, 23, 1355–1364, https://doi.org/10.1897/03-420, 2004.

Keyte, I. J., Harrison, R. M., and Lammel, G.: Chemical reactivity and long-range transport potential of polycyclic aromatic hydrocarbons – a review, Chem. Soc. Rev., 42, 9333–9391, https://doi.org/10.1039/C3CS60147A, 2013.

Kim, K.-H., Jahan, S. A., Kabir, E., and Brown, R. J. C.: A review of airborne polycyclic aromatic hydrocarbons (PAHs) and their human health effects, Environment international, 60, 71–80, https://doi.org/10.1016/j.envint.2013.07.019, 2013.

Köllner, F., Schneider, J., Willis, M. D., Klimach, T., Helleis, F., Bozem, H., Kunkel, D., Hoor, P., Burkart, J., Leaitch, W. R., Aliabadi, A. A., Abbatt, J. P. D., Herber, A. B., and Borrmann, S.: Particulate trimethylamine in the summertime Canadian high Arctic lower troposphere, Atmos. Chem. Phys., 17, 13747–13766, https://doi.org/10.5194/acp-17-13747-2017, 2017.

Kruth, C., Czech, H., Sklorz, M., Passig, J., Ehlert, S., Cappiello, A., and Zimmermann, R.: Direct Infusion Resonance-Enhanced Multiphoton Ionization Mass Spectrometry of Liquid Samples under Vacuum Conditions, Anal. Chem., 89, 10917–10923, https://doi.org/10.1021/acs.analchem.7b02633, 2017.

Lacher, L., Clemen, H.-C., Shen, X., Mertes, S., Gysel-Beer, M., Moallemi, A., Steinbacher, M., Henne, S., Saathoff, H., Möhler, O., Höhler, K., Schiebel, T., Weber, D., Schrod, J., Schneider, J., and Kanji, Z. A.: Sources and nature of ice-nucleating particles in the free troposphere at Jungfraujoch in winter 2017, Atmos. Chem. Phys., 21, 16925–16953, https://doi.org/10.5194/acp-21-16925-2021, available at: https://acp.copernicus.org/articles/21/16925/2021/, 2021.

Lähteenmäki-Uutela, A., Yliskylä-Peuralahti, J., Repka, S., and Mellqvist, J.: What explains SECA compliance: rational calculation or moral judgment?, WMU J Marit Affairs, 18, 61–78, https://doi.org/10.1007/s13437-019-00163-1, 2019.

Laskin, J., Laskin, A., and Nizkorodov, S. A.: Mass Spectrometry Analysis in Atmospheric Chemistry, Anal. Chem., 90, 166–189, https://doi.org/10.1021/acs.analchem.7b04249, 2018.

Lee, A. K. Y., Willis, M. D., Healy, R. M., Wang, J. M., Jeong, C.-H., Wenger, J. C., Evans, G. J., and Abbatt, J. P. D.: Single-particle characterization of biomass burning organic aerosol (BBOA): evidence for non-uniform mixing of high molecular weight organics and potassium, Atmos. Chem. Phys., 16, 5561–5572, https://doi.org/10.5194/acp-16-5561-2016, 2016.

Li, C., He, Q., Schade, J., Passig, J., Zimmermann, R., Meidan, D., Laskin, A., and Rudich, Y.: Dynamic changes in optical and chemical properties of tar ball aerosols by atmospheric photochemical aging, Atmospheric Chemistry and Physics, 19, 139–163, https://doi.org/10.5194/acp-19-139-2019, 2019.

Li, L., Liu, L., Xu, L., Li, M., Li, X., Gao, W., Huang, Z., and Cheng, P.: Improvement in the Mass Resolution of Single Particle Mass Spectrometry Using Delayed Ion Extraction, Journal of the American Society for Mass Spectrometry, 29, 2105–2109, https://doi.org/10.1007/s13361-018-2037-4, 2018.

Lima, A. L. C., Farrington, J. W., and Reddy, C. M.: Combustion-Derived Polycyclic Aromatic Hydrocarbons in the Environment—A Review, Environmental Forensics, 6, 109–131, https://doi.org/10.1080/15275920590952739, 2005.

Ma, L., Li, M., Zhang, H., Li, L., Huang, Z., Gao, W., Chen, D., Fu, Z., Nian, H., Zou, L., Gao, J., Chai, F., and Zhou, Z.: Comparative analysis of chemical composition and sources of aerosol particles in urban Beijing during clear, hazy, and dusty days using single particle aerosol mass spectrometry, J. Clean. Prod., 112, 1319–1329, https://doi.org/10.1016/j.jclepro.2015.04.054, 2016.

Marsden, N. A., Flynn, M. J., Allan, J. D., and Coe, H.: Online differentiation of mineral phase in aerosol particles by ion formation mechanism using a LAAP-TOF single-particle mass spectrometer, Atmos. Meas. Tech., 11, 195–213, https://doi.org/10.5194/amt-11-195-2018, available at: https://amt.copernicus.org/articles/11/195/2018/, 2018.

Middlebrook, A. M., Murphy, D. M., and Thomson, D. S.: Observations of organic material in individual marine particles at Cape Grim during the First Aerosol Characterization Experiment (ACE 1), J. Geophys. Res., 103, 16475–16483, https://doi.org/10.1029/97JD03719, 1998.

Miersch, T., Czech, H., Stengel, B., Abbaszade, G., Orasche, J., Sklorz, M., Streibel, T., and Zimmermann, R.: Composition of carbonaceous fine particulate emissions of a flexible fuel DISI engine under high velocity and municipal conditions, Fuel, 236, 1465–1473, https://doi.org/10.1016/j.fuel.2018.09.136, 2019.

Moldanová, J., Fridell, E., Popovicheva, O., Demirdjian, B., Tishkova, V., Faccinetto, A., and Focsa, C.: Characterisation of particulate matter and gaseous emissions from a large ship diesel engine, Atmospheric Environ., 43, 2632–2641, https://doi.org/10.1016/j.atmosenv.2009.02.008, 2009.

Morrical, B. D., Fergenson, D. P., and Prather, K. A.: Coupling two-step laser desorption/ionization with aerosol time-of-flight mass spectrometry for the analysis of individual organic particles, J. Am. Soc. Mass Spectrom., 9, 1068–1073, https://doi.org/10.1016/S1044-0305(98)00074-9, 1998.

Murphy, D. M., Cziczo, D. J., Froyd, K. D., Hudson, P. K., Matthew, B. M., Middlebrook, A. M., Peltier, R. E., Sullivan, A., Thomson, D. S., and Weber, R. J.: Single-particle mass spectrometry of tropospheric aerosol particles, J. Geophys. Res., 111, n/a-n/a, https://doi.org/10.1029/2006JD007340, 2006.

Murphy, D. M.: The design of single particle laser mass spectrometers, Mass Spectrom. Rev., 26, 150–165, https://doi.org/10.1002/mas.20113, 2007.

Murphy, D. M., Froyd, K. D., Bian, H., Brock, C. A., Dibb, J. E., DiGangi, J. P., Diskin, G., Dollner, M., Kupc, A., Scheuer, E. M., Schill, G. P., Weinzierl, B., Williamson, C. J., and Yu, P.: The distribution of sea-salt aerosol in the global troposphere, Atmos. Chem. Phys., 19, 4093–4104, https://doi.org/10.5194/acp-19-4093-2019, 2019.

Nash, D. G., Liu, X. F., Mysak, E. R., and Baer, T.: Aerosol particle mass spectrometry with low photon energy laser ionization, Int. J. Mass Spectrom., 241, 89–97, https://doi.org/10.1016/j.ijms.2004.12.016, 2005.

Neubauer, K. R., Johnston, M. V., and Wexler, A. S.: Humidity effects on the mass spectra of single aerosol particles, Atmospheric Environ., 32, 2521–2529, https://doi.org/10.1016/S1352-2310(98)00005-3, 1998.

Nguyen, D.-L., Czech, H., Pieber, S. M., Schnelle-Kreis, J., Steinbacher, M., Orasche, J., Henne, S., Popovicheva, O. B., Abbaszade, G., Engling, G., Bukowiecki, N., Nguyen, N.-A., Nguyen, X.-A., and Zimmermann, R.: Carbonaceous aerosol composition in air masses influenced by large-scale biomass burning: a case study in northwestern Vietnam, Atmos. Chem. Phys., 21, 8293–8312, https://doi.org/10.5194/acp-21-8293-2021, 2021.

Nozière, B., Kalberer, M., Claeys, M., Allan, J., D'Anna, B., Decesari, S., Finessi, E., Glasius, M., Grgić, I., Hamilton, J. F., Hoffmann, T., Iinuma, Y., Jaoui, M., Kahnt, A., Kampf, C. J., Kourtchev, I., Maenhaut, W., Marsden, N., Saarikoski, S., Schnelle-Kreis, J., Surratt, J. D., Szidat, S., Szmigielski, R., and Wisthaler, A.: The molecular identification of organic

compounds in the atmosphere: state of the art and challenges, Chem. Rev., 115, 3919–3983, https://doi.org/10.1021/cr5003485, 2015.

Oster, M., Elsasser, M., Schnelle-Kreis, J., and Zimmermann, R.: First field application of a thermal desorption resonance-enhanced multiphoton-ionisation single particle time-of-flight mass spectrometer for the on-line detection of particle-bound polycyclic aromatic hydrocarbons, Anal. Bioanal. Chem., 401, 3173–3182, https://doi.org/10.1007/s00216-011-5438-9, available at: https://doi.org/10.1007/s00216-011-5438-9, 2011.

Pandey, S. K., Kim, K.-H., and Brown, R. J.: A review of techniques for the determination of polycyclic aromatic hydrocarbons in air, TrAC Trends in Analytical Chemistry, 30, 1716–1739, https://doi.org/10.1016/j.trac.2011.06.017, 2011.

Passig, J., Schade, J., Irsig, R., Li, L., Li, X., Zhou, Z., Adam, T., and Zimmermann, R.: Detection of Ship Plumes from Residual Fuel Operation in Emission Control Areas using Single-Particle Mass Spectrometry, Atmospheric Measurement Techniques, 2021, 4171–4185, https://doi.org/10.5194/amt-14-4171-2021, 2021.

Passig, J., Schade, J., Rosewig, E. I., Irsig, R., Kröger-Badge, T., Czech, H., Sklorz, M., Streibel, T., Li, L., Li, X., Zhou, Z., Fallgren, H., Moldanova, J., and Zimmermann, R.: Resonance-enhanced detection of metals in aerosols using single-particle mass spectrometry, Atmos. Chem. Phys., 20, 7139–7152, https://doi.org/10.5194/acp-20-7139-2020, 2020.

Passig, J. and Zimmermann, R.: Laser Ionization in Single-Particle Mass Spectrometry, in: Photoionization and Photo-Induced Processes in Mass Spectrometry: Fundamentals and Applications, edited by: Zimmermann, R. and Hanley, L., Wiley-VCH, Weinheim, https://doi.org/10.1002/9783527682201.ch11, 2020.

Passig, J., Schade, J., Oster, M., Fuchs, M., Ehlert, S., Jäger, C., Sklorz, M., and Zimmermann, R.: Aerosol Mass Spectrometer for Simultaneous Detection of Polyaromatic Hydrocarbons and Inorganic Components from Individual Particles, Anal. Chem., 89, 6341–6345, https://doi.org/10.1021/acs.analchem.7b01207, 2017.

Phousongphouang, P. T. and Arey, J.: Rate Constants for the Gas-Phase Reactions of a Series of Alkylnaphthalenes with the OH Radical, Environ. Sci. Technol., 36, 1947–1952, https://doi.org/10.1021/es011434c, 2002.

Pöschl, U. and Shiraiwa, M.: Multiphase chemistry at the atmosphere-biosphere interface influencing climate and public health in the anthropocene, Chem. Rev., 115, 4440–4475, https://doi.org/10.1021/cr500487s, 2015.

Prather, K. A., Nordmeyer, T., and Salt, K.: Real-time characterization of individual aerosol particles using time-of-flight mass spectrometry, Anal. Chem., 66, 1403–1407, https://doi.org/10.1021/ac00081a007, 1994.

Pratt, K. A. and Prather, K. A.: Mass spectrometry of atmospheric aerosols--recent developments and applications. Part II: On-line mass spectrometry techniques, Mass Spectrom. Rev., 31, 17–48, https://doi.org/10.1002/mas.20330, 2012.

Ravindra, K., Sokhi, R., and van Grieken, R.: Atmospheric polycyclic aromatic hydrocarbons: Source attribution, emission factors and regulation, Atmospheric Environ., 42, 2895–2921, https://doi.org/10.1016/j.atmosenv.2007.12.010, 2008.

Reinard, M. S. and Johnston, M. V.: Ion formation mechanism in laser desorption ionization of individual nanoparticles, Journal of the American Society for Mass Spectrometry, 19, 389–399, https://doi.org/10.1016/j.jasms.2007.11.017, 2008.

Riemer, N., Ault, A. P., West, M., Craig, R. L., and Curtis, J. H.: Aerosol Mixing State: Measurements, Modeling, and Impacts, Rev. Geophys., 57, 187–249, https://doi.org/10.1029/2018RG000615, 2019.

Riva, M., Heikkinen, L., Bell, D. M., Peräkylä, O., Zha, Q., Schallhart, S., Rissanen, M. P., Imre, D., Petäjä, T., Thornton, J. A., Zelenyuk, A., and Ehn, M.: Chemical transformations in monoterpene-derived organic aerosol enhanced by inorganic composition, npj Climate and Atmospheric Science, 2, 2, https://doi.org/10.1038/s41612-018-0058-0, 2019.

Romay, F. J., Roberts, D. L., Marple, V. A., Liu, B. Y. H., and Olson, B. A.: A High-Performance Aerosol Concentrator for Biological Agent Detection, Aerosol Sci. Technol., 36, 217–226, https://doi.org/10.1080/027868202753504074, 2002.

Sakurai, H., Tobias, H. J., Park, K., Zarling, D., Docherty, K. S., Kittelson, D. B., McMurry, P. H., and Ziemann, P. J.: On-line measurements of diesel nanoparticle composition and volatility, Atmospheric Environ., 37, 1199–1210, https://doi.org/10.1016/S1352-2310(02)01017-8, 2003.

Schade, J., Passig, J., Irsig, R., Ehlert, S., Sklorz, M., Adam, T., Li, C., Rudich, Y., and Zimmermann, R.: Spatially Shaped Laser Pulses for the Simultaneous Detection of Polycyclic Aromatic Hydrocarbons as well as Positive and Negative Inorganic Ions in Single Particle Mass Spectrometry, Analytical chemistry, 91, 10282–10288, https://doi.org/10.1021/acs.analchem.9b02477, 2019.

Schmidt, S., Schneider, J., Klimach, T., Mertes, S., Schenk, L. P., Kupiszewski, P., Curtius, J., and Borrmann, S.: Online single particle analysis of ice particle residuals from mountain-top mixed-phase clouds using laboratory derived particle type assignment, Atmos. Chem. Phys., 17, 575–594, https://doi.org/10.5194/acp-17-575-2017, available at: https://acp.copernicus.org/articles/17/575/2017/, 2017.

Shen, X., Saathoff, H., Huang, W., Mohr, C., Ramisetty, R., and Leisner, T.: Understanding atmospheric aerosol particles with improved particle identification and quantification by single-particle mass spectrometry, Atmos. Meas. Tech., 12, 2219–2240, https://doi.org/10.5194/amt-12-2219-2019, 2019a.

Shen, X., Vogel, H., Vogel, B., Huang, W., Mohr, C., Ramisetty, R., Leisner, T., Prévôt, A. S. H., and Saathoff, H.: Composition and origin of PM2.5 aerosol particles in the upper Rhine valley in summer, Atmos. Chem. Phys., 19, 13189–13208, https://doi.org/10.5194/acp-19-13189-2019, 2019b.

Shen, X., Ramisetty, R., Mohr, C., Huang, W., Leisner, T., and Saathoff, H.: Laser ablation aerosol particle time-of-flight mass spectrometer (LAAPTOF): performance, reference spectra and classification of atmospheric samples, Atmos. Meas. Tech., 11, 2325–2343, https://doi.org/10.5194/amt-11-2325-2018, 2018.

Shrivastava, M., Lou, S., Zelenyuk, A., Easter, R. C., Corley, R. A., Thrall, B. D., Rasch, P. J., Fast, J. D., Simonich, S. L. M., Shen, H., and Tao, S.: Global long-range transport and lung cancer risk from polycyclic aromatic hydrocarbons shielded by coatings of organic aerosol, PNAS, 114, 1246–1251, https://doi.org/10.1073/pnas.1618475114, 2017.

Silva, P. J. and Prather, K. A.: Interpretation of Mass Spectra from Organic Compounds in Aerosol Time-of-Flight Mass Spectrometry, Anal. Chem., 72, 3553–3562, https://doi.org/10.1021/ac9910132, 2000.

Silva, P. J., Liu, D.-Y., Noble, C. A., and Prather, K. A.: Size and Chemical Characterization of Individual Particles Resulting from Biomass Burning of Local Southern California Species, Environ. Sci. Technol., 33, 3068–3076, https://doi.org/10.1021/es980544p, 1999.

SMHI: Sveriges meteorologiska och hydrologiska institut, https://www.smhi.se/data/meteorologi/ladda-ner-meteorologiska-observationer#param=airtemperatureInstant,stations=all,stationid=71190, last access: 14 January 2021, 2021.

Sodeman, D. A., Toner, S. M., and Prather, K. A.: Determination of Single Particle Mass Spectral Signatures from Light-Duty Vehicle Emissions, Environ. Sci. Technol., 39, 4569–4580, https://doi.org/10.1021/es0489947, 2005.

Song, X.-H., Hopke, P. K., Fergenson, D. P., and Prather, K. A.: Classification of Single Particles Analyzed by ATOFMS Using an Artificial Neural Network, ART-2A, Anal. Chem., 71, 860–865, https://doi.org/10.1021/ac9809682, 1999.

Spencer, M. T. and Prather, K. A.: Using ATOFMS to Determine OC/EC Mass Fractions in Particles, Aerosol Sci. Technol., 40, 585–594, https://doi.org/10.1080/02786820600729138, 2006.

Spencer, M. T., Shields, L. G., Sodeman, D. A., Toner, S. M., and Prather, K. A.: Comparison of oil and fuel particle chemical signatures with particle emissions from heavy and light duty vehicles, Atmospheric Environ., 40, 5224–5235, https://doi.org/10.1016/j.atmosenv.2006.04.011, 2006.

Stein, A. F., Draxler, R. R., Rolph, G. D., Stunder, B. J. B., Cohen, M. D., and Ngan, F.: NOAA's HYSPLIT Atmospheric Transport and Dispersion Modeling System, Bulletin of the American Meteorological Society, 96, 2059–2077, https://doi.org/10.1175/BAMS-D-14-00110.1, 2015.

Streibel, T., Schnelle-Kreis, J., Czech, H., Harndorf, H., Jakobi, G., Jokiniemi, J., Karg, E., Lintelmann, J., Matuschek, G., Michalke, B., Müller, L., Orasche, J., Passig, J., Radischat, C., Rabe, R., Reda, A., Rüger, C., Schwemer, T., Sippula, O., Stengel, B., Sklorz, M., Torvela, T., Weggler, B., and Zimmermann, R.: Aerosol emissions of a ship diesel engine operated with diesel fuel or heavy fuel oil, Environmental Science and Pollution Research, 24, 10976–10991, https://doi.org/10.1007/s11356-016-6724-z, 2017.

Su, Y., Sipin, M. F., Furutani, H., and Prather, K. A.: Development and characterization of an aerosol time-of-flight mass spectrometer with increased detection efficiency, Analytical chemistry, 76, 712–719, https://doi.org/10.1021/ac034797z, 2004.

Sullivan, R. C., Guazzotti, S. A., Sodeman, D. A., and Prather, K. A.: Direct observations of the atmospheric processing of Asian mineral dust, Atmos. Chem. Phys., 7, 1213–1236, https://doi.org/10.5194/acp-7-1213-2007, 2007.

Sultana, C. M., Cornwell, G. C., Rodriguez, P., and Prather, K. A.: FATES: a flexible analysis toolkit for the exploration of single-particle mass spectrometer data, Atmos. Meas. Tech., 10, 1323–1334, https://doi.org/10.5194/amt-10-1323-2017, 2017.

Sykes, D. C., Woods, E., Smith, G. D., Baer, T., and Miller, R. E.: Thermal Vaporization-Vacuum Ultraviolet Laser Ionization Time-of-Flight Mass Spectrometry of Single Aerosol Particles, Anal. Chem., 74, 2048–2052, https://doi.org/10.1021/ac011225a, 2002.

Tobiszewski, M. and Namieśnik, J.: PAH diagnostic ratios for the identification of pollution emission sources, Environmental Pollution, 162, 110–119, https://doi.org/10.1016/j.envpol.2011.10.025, 2012.

Toner, S. M., Shields, L. G., Sodeman, D. A., and Prather, K. A.: Using mass spectral source signatures to apportion exhaust particles from gasoline and diesel powered vehicles in a freeway study using UF-ATOFMS, Atmospheric Environ., 42, 568–581, https://doi.org/10.1016/j.atmosenv.2007.08.005, 2008.

Toner, S. M., Sodeman, D. A., and Prather, K. A.: Single Particle Characterization of Ultrafine and Accumulation Mode Particles from Heavy Duty Diesel Vehicles Using Aerosol Time-of-Flight Mass Spectrometry, Environ. Sci. Technol., 40, 3912–3921, https://doi.org/10.1021/es051455x, 2006.

Vera, C. C., Trimborn, A., Hinz, K.-P., and Spengler, B.: Initial velocity distributions of ions generated by in-flight laser desorption/ionization of individual polystyrene latex microparticles as studied by the delayed ion extraction method, Rapid communications in mass spectrometry RCM, 19, 133–146, https://doi.org/10.1002/rcm.1753, 2005.

Vereecken, L.: Reaction Mechanisms for the Atmospheric Oxidation of Monocyclic Aromatic Compounds, in: Advances in Atmospheric Chemistry, edited by: Barker, J. R. and Steiner, A. L., WORLD SCIENTIFIC, 377–527, https://doi.org/10.1142/9789813271838_0006, 2018.

Vione, D., Maurino, V., Minero, C., Pelizzetti, E., Harrison, M. A. J., Olariu, R.-I., and Arsene, C.: Photochemical reactions in the tropospheric aqueous phase and on particulate matter, Chem. Soc. Rev., 35, 441–453, https://doi.org/10.1039/B510796M, 2006.

Wang, S., Zordan, C. A., and Johnston, M. V.: Chemical characterization of individual, airborne sub-10-nm particles and molecules, Anal. Chem., 78, 1750–1754, https://doi.org/10.1021/ac052243l, 2006.

Wang, X., Shen, Y., Lin, Y., Pan, J., Zhang, Y., Louie, P. K. K., Li, M., and Fu, Q.: Atmospheric pollution from ships and its impact on local air quality at a port site in Shanghai, Atmos. Chem. Phys., 19, 6315–6330, https://doi.org/10.5194/acp-19-6315-2019, available at: https://acp.copernicus.org/articles/19/6315/2019/, 2019.

Wang, X., Gao, S., Yang, X., Chen, H., Chen, J., Zhuang, G., Surratt, J. D., Chan, M. N., and Seinfeld, J. H.: Evidence for high molecular weight nitrogen-containing organic salts in urban aerosols, Environ. Sci. Technol., 44, 4441–4446, https://doi.org/10.1021/es1001117, 2010.

Wilkerson, C. W., Colby, S. M., and Reilly, J. P.: Determination of polycyclic aromatic hydrocarbons using gas chromatography/laser ionization mass spectrometry with picosecond and nanosecond light pulses, Anal. Chem., 61, 2669–2673, https://doi.org/10.1021/ac00198a016, 1989.

Woods, E., Smith, G. D., Dessiaterik, Y., Baer, T., and Miller, R. E.: Quantitative Detection of Aromatic Compounds in Single Aerosol Particle Mass Spectrometry, Anal. Chem., 73, 2317–2322, https://doi.org/10.1021/ac001166l, 2001.

Xu, J., Wang, H., Li, X., Li, Y., Wen, J., Zhang, J., Shi, X., Li, M., Wang, W., Shi, G., and Feng, Y.: Refined source apportionment of coal combustion sources by using single particle mass spectrometry, Sci. Total Environ., 627, 633–646, https://doi.org/10.1016/j.scitotenv.2018.01.269, 2018.

Zelenyuk, A. and Imre, D.: Single Particle Laser Ablation Time-of-Flight Mass Spectrometer: An Introduction to SPLAT, Aerosol Science and Technology, 39, 554–568, https://doi.org/10.1080/027868291009242, 2005.

Zelenyuk, A., Imre, D. G., Wilson, J., Bell, D. M., Suski, K. J., Shrivastava, M., Beránek, J., Alexander, M. L., Kramer, A. L., and Massey Simonich, S. L.: The effect of gas-phase polycyclic aromatic hydrocarbons on the formation and properties of biogenic secondary organic aerosol particles, Faraday discussions, 200, 143–164, https://doi.org/10.1039/c7fd00032d, 2017.

Zelenyuk, A., Imre, D., Beránek, J., Abramson, E., Wilson, J., and Shrivastava, M.: Synergy between secondary organic aerosols and long-range transport of polycyclic aromatic hydrocarbons, Environ. Sci. Technol., 46, 12459–12466, https://doi.org/10.1021/es302743z, 2012.

Zelenyuk, A., Yang, J., Choi, E., and Imre, D.: SPLAT II: An Aircraft Compatible, Ultra-Sensitive, High Precision Instrument for In-Situ Characterization of the Size and Composition of Fine and Ultrafine Particles, Aerosol Science and Technology, 43, 411–424, https://doi.org/10.1080/02786820802709243, 2009.

Zhang, G., Bi, X., Li, L., Chan, L. Y., Li, M., Wang, X., Sheng, G., Fu, J., and Zhou, Z.: Mixing state of individual submicron carbon-containing particles during spring and fall seasons in urban Guangzhou, China: a case study, Atmos. Chem. Phys., 13, 4723–4735, https://doi.org/10.5194/acp-13-4723-2013, 2013.

Zhang, W., Zhang, S., Wan, C., Yue, D., Ye, Y., and Wang, X.: Source diagnostics of polycyclic aromatic hydrocarbons in urban road runoff, dust, rain and canopy throughfall, Environmental Pollution, 153, 594–601, https://doi.org/10.1016/j.envpol.2007.09.004, 2008.

Zhou, L., Hopke, P. K., and Venkatachari, P.: Cluster analysis of single particle mass spectra measured at Flushing, NY, Analytica Chimica Acta, 555, 47–56, https://doi.org/10.1016/j.aca.2005.08.061, available at: http://www.sciencedirect.com/science/article/pii/S0003267005014649, 2006.

Zhou, Y., Huang, X. H., Griffith, S. M., Li, M., Li, L., Zhou, Z., Wu, C., Meng, J., Chan, C. K., Louie, P. K., and Yu, J. Z.: A field measurement based scaling approach for quantification of major ions, organic carbon, and elemental carbon using a single particle aerosol mass spectrometer, Atmospheric Environ., 143, 300–312, https://doi.org/10.1016/j.atmosenv.2016.08.054, 2016.

Zhuo, Z., Su, B., Xie, Q., Li, L., Huang, Z., Zhou, Z., Mai, Z., and Tan, G.: Improved Aerodynamic Particle Concentrator for Single Particle Aerosol Mass Spectrometry: A Simulation and Characterization Study, Chinese Journal of Vacuum Science and Technology, 443–449, https://doi.org/10.13922/j.cnki.cjvst.202008026, 2021.

Zimmermann, R., Ferge, T., Gälli, M., and Karlsson, R.: Application of single-particle laser desorption/ionization time-of-flight mass spectrometry for detection of polycyclic aromatic hydrocarbons from soot particles originating from an industrial combustion process, Rapid communications in mass spectrometry RCM, 17, 851–859, https://doi.org/10.1002/rcm.979, 2003.

Zimmermann, R. and Hanley, L. (Eds.): Photoionization and Photo-Induced Processes in Mass Spectrometry: Fundamentals and Applications, Wiley-VCH, Weinheim, 2020.